The interplay between theory and computation in the study of 3D Euler equations

Thomas Y. Hou

Applied and Computational Mathematics
California Institute of Technology

Joint work with Guo Luo and Pengfei Liu

First Annual Meeting of Applied Mathematics, Taida, Dec. 6, 2015

The Basic Problem

The 3D incompressible Euler equations are given by

$$\mathbf{u}_t + \mathbf{u} \cdot \nabla \mathbf{u} = -\nabla p, \qquad \nabla \cdot \mathbf{u} = 0,$$

with initial condition $\mathbf{u}(\mathbf{x}, 0) = \mathbf{u}_0$.

Define vorticity $\omega = \nabla \times \mathbf{u}$, then ω is governed by

$$\omega_t + (\mathbf{u} \cdot \nabla)\omega = \nabla \mathbf{u} \cdot \omega.$$

Note that $\nabla \mathbf{u}$ is related to ω by a Riesz operator K of degree zero: $\nabla \mathbf{u} = K(\omega)$, and we have $\|\omega\|_{L^p} \leq \|\nabla \mathbf{u}\|_{L^p} \leq C\|\omega\|_{L^p}$ for $1 < p < \infty$.

Thus the vortex stretching term $\nabla \mathbf{u} \cdot \omega$ is formally of the order ω^2.

Significance of the Problem

- Why important?
  - The grand open problem: existence or nonexistence of global regular solutions from smooth initial data
  - Closely related to one of the seven Clay Millennium Problems
  - mathematically: the problem remained open for more than 250 years
  - physically: singularity in inviscid flows may (i) signify the onset of turbulence in viscous flows, and (ii) be a mechanism for energy transfer to small scales

Previous Work

- On the theoretical side:
  - Kato (1972): local well-posedness
  - Beale-Kato-Majda (1984): necessary and sufficient blowup criterion
  - Constantin-Fefferman-Majda (1996): geometric constraints for blowup
  - Deng-Hou-Yu (2005): Lagrangian localized geometric constraints
- Other related work:
  - Constantin-Majda-Tabak (1994): 2D surface quasi-geostrophic (SQG) equations as a model for 3D Euler
  - Cordoba (1998): no blowup of 2D SQG near a hyperbolic saddle

Previous Work (Cont'd)

- On the numerical search for singularity:
  - Grauer and Sideris (1991): first numerical study of axisymmetric flows with swirl; blowup reported away from the axis
  - Pumir and Siggia (1992): axisymmetric flows with swirl; blowup reported away from the axis
  - Kerr (1993): antiparallel vortex tubes; blowup reported
  - E and Shu (1994): 2D Boussinesq; no blowup observed
  - Boratav and Pelz (1994): viscous simulations using Kida's high-symmetry initial condition; blowup reported
  - Grauer et al. (1998): perturbed vortex tube; blowup reported
  - Hou and Li (2006): use Kerr's two anti-parallel vortex tube initial data with higher resolution; no blowup observed
  - Orlandi and Carnevale (2007): Lamb dipoles; blowup reported
- Evidence for blowup is inconclusive and problem remains open

Numerical evidence of Euler singularity

In 1993 (and 2005), R. Kerr [Phys. Fluids] presented numerical evidence of 3D Euler singularity for two anti-parallel vortex tubes:

- Pseudo-spectral in x and y, Chebyshev in z direction;
- Best resolution: $512 \times 256 \times 192$;
- Predicted singularity time $T = 18.7$, but his numerical solutions became under-resolved after $T_1 = 17$.
- $\|\boldsymbol{\omega}\|_{L^\infty} \approx (T-t)^{-1}$; $\|\mathbf{u}\|_{L^\infty} \approx (T-t)^{-1/2}$;
- Anisotropic scaling: $(T-t) \times \sqrt{T-t} \times \sqrt{T-t}$;
- Vortex lines: relatively straight, $|\nabla \boldsymbol{\xi}| \approx (T-t)^{-1/2}$;
- It is important to emphasize that $T - T_1 = 1.7$ is not asymptotically small. Thus the extrapolated blow-up rate of $\|\boldsymbol{\omega}\|_{L^\infty} \approx (T-t)^{-1}$ is **not** valid asymptotically from T_1 to T. This makes the claim $\int_{T_1}^{T} \|\omega\|_\infty dt = \infty$ questionable.
- Kerr's computation falls into the critical case of Deng-Hou-Yu's non-blowup criterion with $A = B = 1/2$.

Computation of Hou and Li, J. Nonlinear Science, 2006

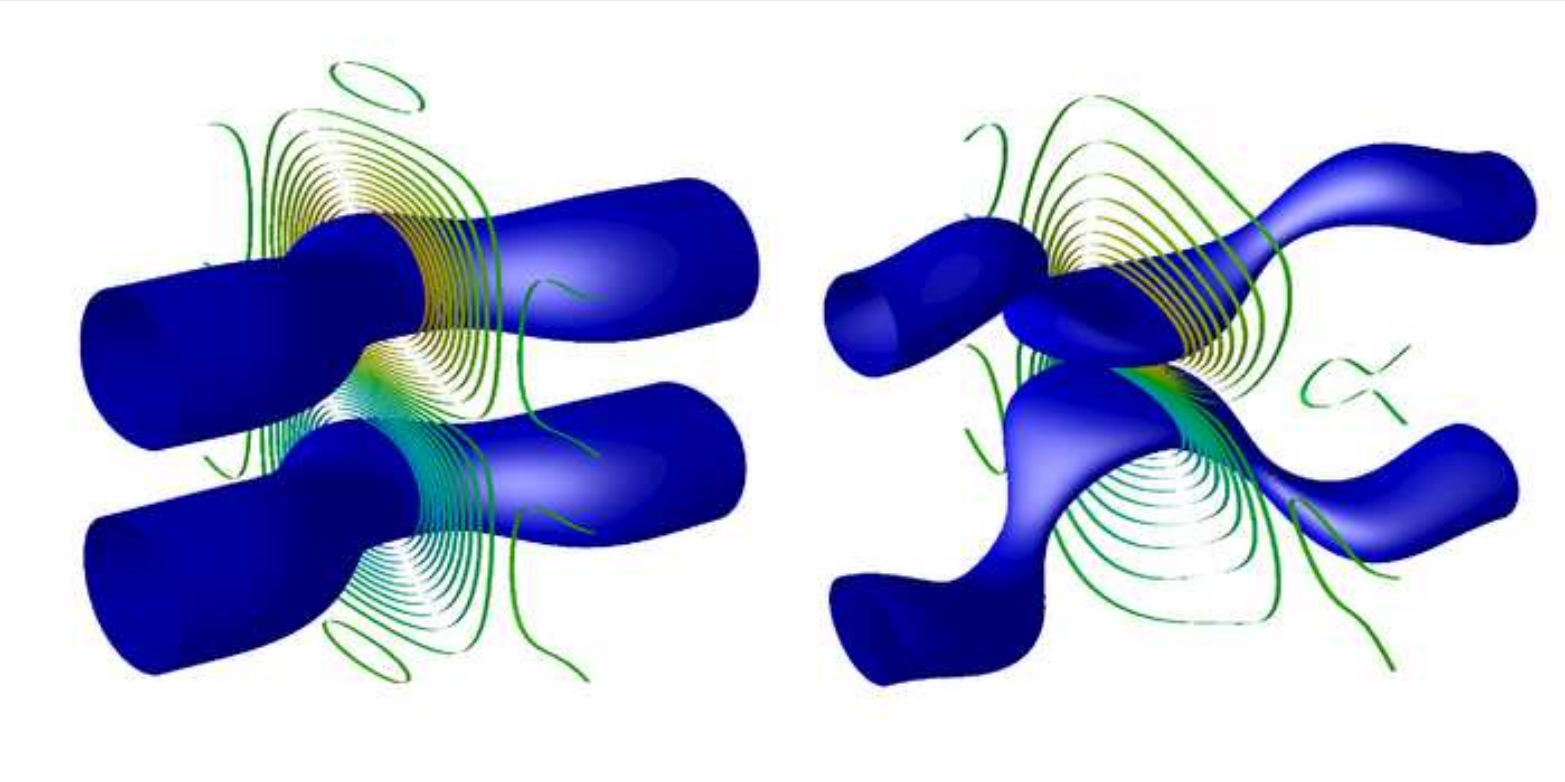

Figure: Two slightly perturbed antiparallel vortex tubes at t=0 and t=6

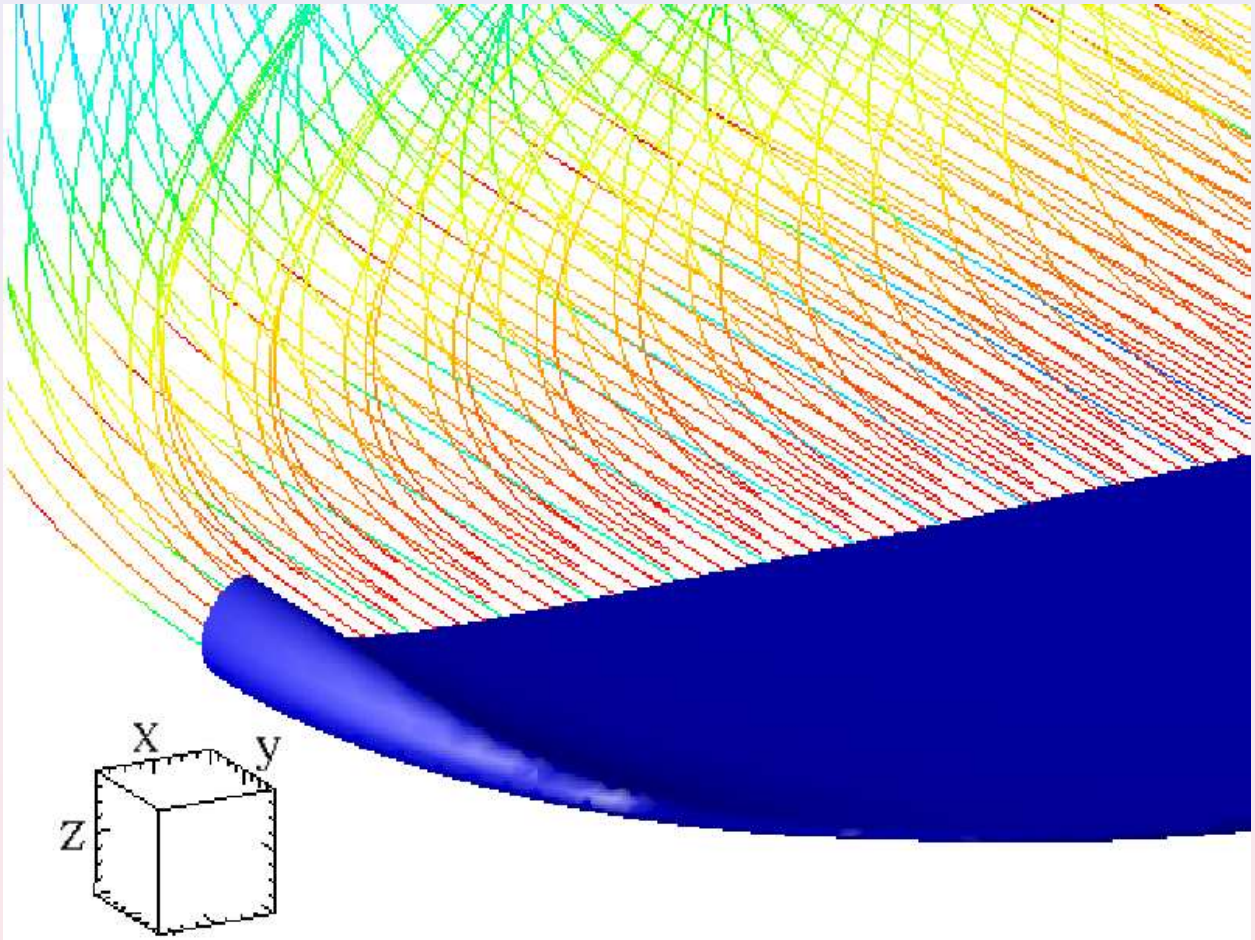

Figure: The local 3D vortex structures and vortex lines around the maximum vorticity at $t = 17$ with resolution $1536 \times 1024 \times 3072$.

Maximum velocity in time

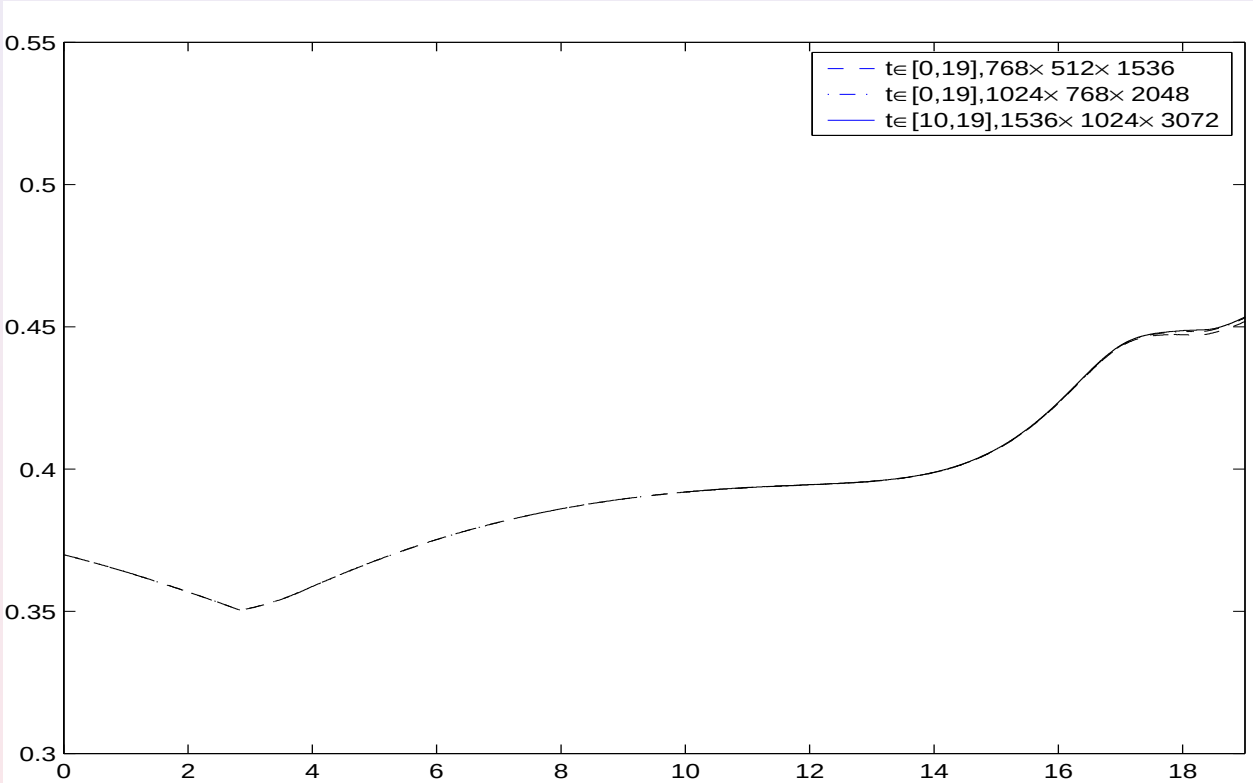

Figure: Maximum velocity $\|\mathbf{u}\|_\infty$ in time using different resolutions. With maximum velocity being bounded, the non-blowup criterion of Deng-Hou-Yu applies with $A = 0$ and $B = 1/2$, implying no blowup at least up to $T = 19$.

Dynamic depletion of vortex stretching

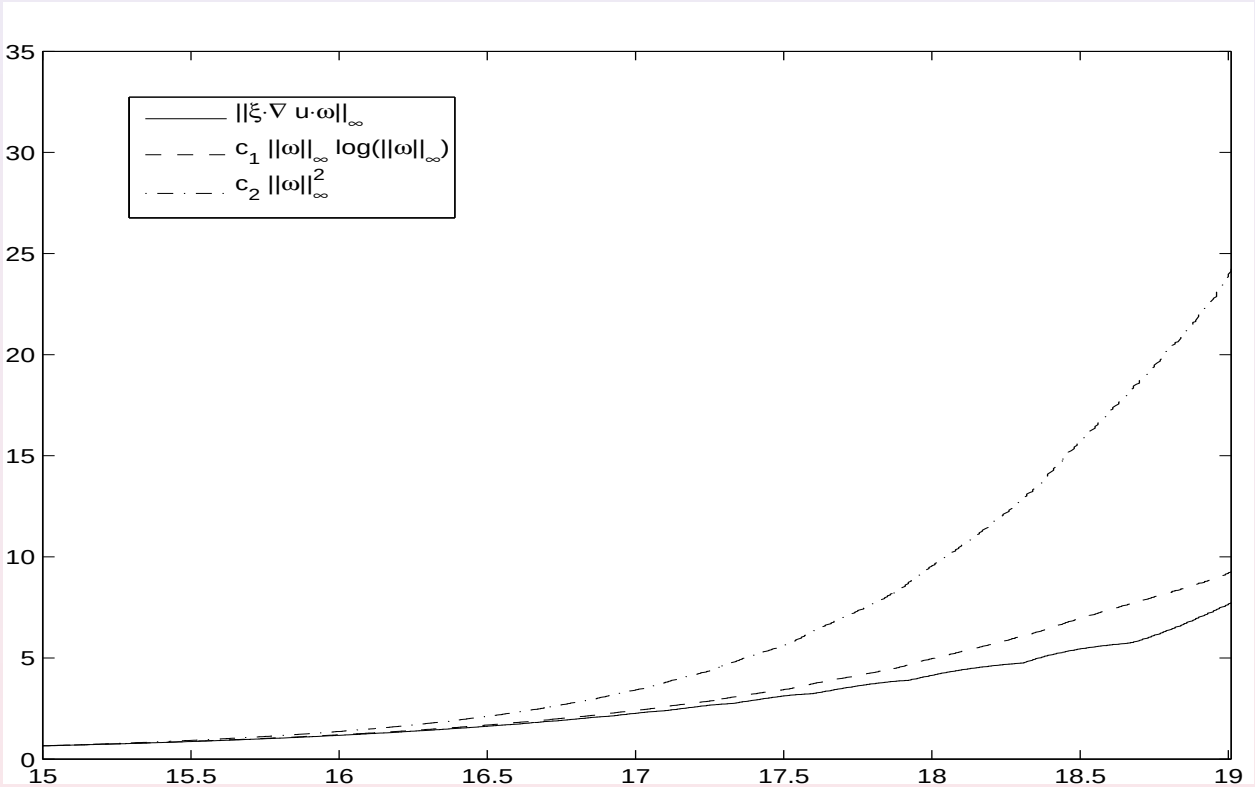

Figure: Study of the vortex stretching term in time, resolution $1536 \times 1024 \times 3072$. The fact $|\boldsymbol{\xi} \cdot \nabla \mathbf{u} \cdot \boldsymbol{\omega}| \leq c_1 |\boldsymbol{\omega}| \log |\boldsymbol{\omega}|$ plus $\frac{D}{Dt}|\omega| = \boldsymbol{\xi} \cdot \nabla \mathbf{u} \cdot \boldsymbol{\omega}$ implies $|\boldsymbol{\omega}|$ bounded by doubly exponential.

Log log plot of maximum vorticity in time

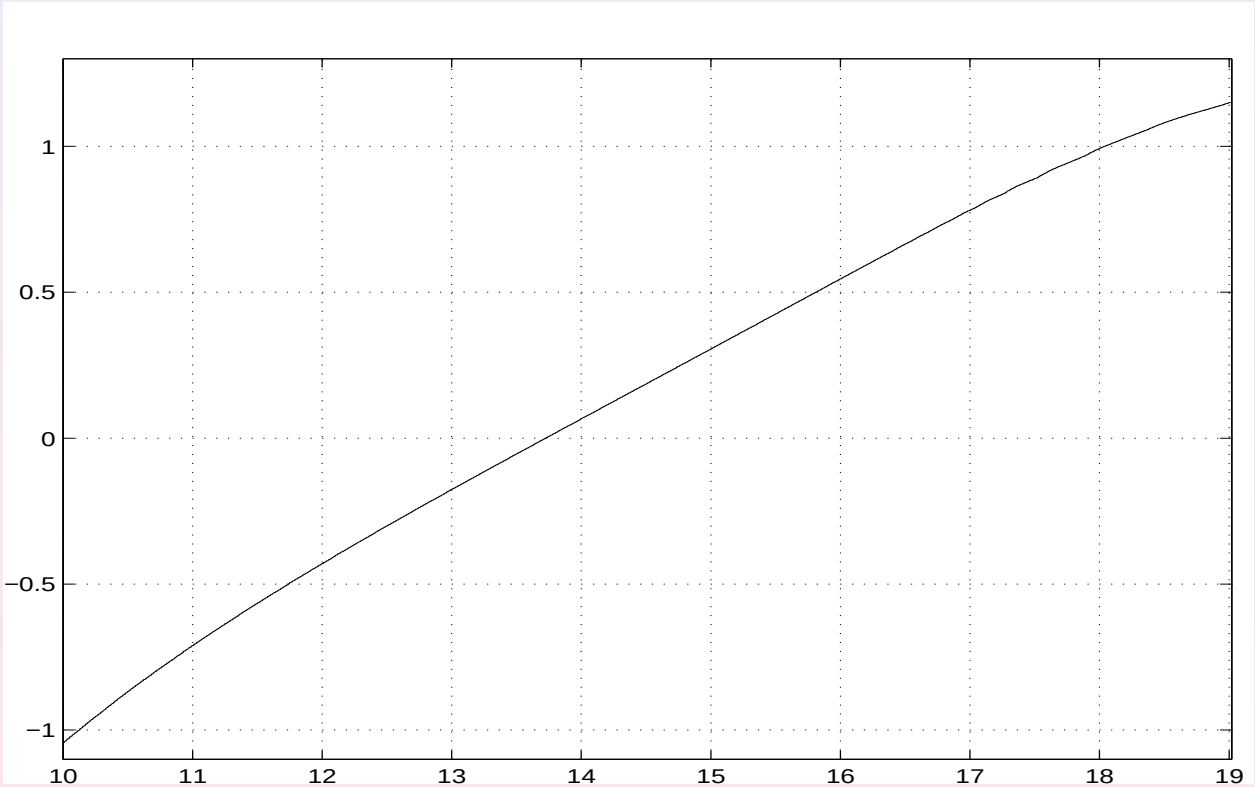

Figure: The plot of $\log\log \|\omega\|_\infty$ vs time, resolution $1536 \times 1024 \times 3072$.

The role of convection in 3D Euler and Navier-Stokes

In [CPAM 08], Hou and Li studied the role of convection for 3D axisymmetric flow and introduced the following new variables:

$$u_1 = u^\theta/r, \quad \omega_1 = \omega^\theta/r, \quad \psi_1 = \psi^\theta/r, \tag{1}$$

and derived the following equivalent system that governs the dynamics of u_1, ω_1 and ψ_1 as follows:

$$\begin{cases} \partial_t u_1 + u^r \partial_r u_1 + u^z \partial_z u_1 = \nu\left(\partial_r^2 + \frac{3}{r}\partial_r + \partial_z^2\right) u_1 + 2u_1\psi_{1z}, \\ \partial_t \omega_1 + u^r \partial_r \omega_1 + u^z \partial_z \omega_1 = \nu\left(\partial_r^2 + \frac{3}{r}\partial_r + \partial_z^2\right)\omega_1 + \left(u_1^2\right)_z, \\ -\left(\partial_r^2 + \frac{3}{r}\partial_r + \partial_z^2\right)\psi_1 = \omega_1, \end{cases} \tag{2}$$

where $u^r = -r\psi_{1z}, \quad u^z = 2\psi_1 + r\psi_{1r}.$

Liu and Wang [SINUM07] showed that if **u** is a smooth velocity field, then u^θ, ω^θ and ψ^θ must satisfy: $u^\theta\big|_{r=0} = \omega^\theta\big|_{r=0} = \psi^\theta\big|_{r=0} = 0$. Thus u_1, ψ_1 and ω_1 are well defiend.

An exact 1D model for 3D Euler/Navier-Stokes

In [Hou-Li, CPAM, **61** (2008), no. 5, 661–697], we derived an excact 1D model along the z-axis for the Navier-Stokes equations:

$$(u_1)_t + 2\psi_1 (u_1)_z = \nu (u_1)_{zz} + 2 (\psi_1)_z u_1, \tag{3}$$

$$(\omega_1)_t + 2\psi_1 (\omega_1)_z = \nu (\omega_1)_{zz} + \left(u_1^2\right)_z, \tag{4}$$

$$-(\psi_1)_{zz} = \omega_1. \tag{5}$$

Let $\tilde{u} = u_1$, $\tilde{v} = -(\psi_1)_z$, and $\tilde{\psi} = \psi_1$. The above system becomes

$$(\tilde{u})_t + 2\tilde{\psi}(\tilde{u})_z = \nu(\tilde{u})_{zz} - 2\tilde{v}\tilde{u}, \tag{6}$$

$$(\tilde{v})_t + 2\tilde{\psi}(\tilde{v})_z = \nu(\tilde{v})_{zz} + (\tilde{u})^2 - (\tilde{v})^2 + c(t), \tag{7}$$

where $\tilde{v} = -(\tilde{\psi})_z$, $\tilde{v}_z = \tilde{\omega}$, and $c(t)$ is an integration constant to enforce the mean of $\tilde{v}$ equal to zero.

The 1D model is exact!

A surprising result is that the above 1D model is exact.

Theorem 1. Let u_1, ψ_1 and ω_1 be the solution of the 1D model (3)-(5) and define

$$u^\theta(r,z,t) = ru_1(z,t), \quad \omega^\theta(r,z,t) = r\omega_1(z,t), \quad \psi^\theta(r,z,t) = r\psi_1(z,t).$$

Then $(u^\theta(r,z,t),\ \omega^\theta(r,z,t),\ \psi^\theta(r,z,t))$ is an exact solution of the 3D Navier-Stokes equations.

Theorem 1 tells us that the 1D model (3)-(5) preserves some essential nonlinear structure of the 3D axisymmetric Navier-Stokes equations.

Global Well-Posedness of the full 1D Model

Theorem 2. *Assume that* $\tilde{u}(z,0)$ *and* $\tilde{v}(z,0)$ *are in* $C^m[0,1]$ *with* $m \geq 1$ *and periodic with period 1. Then the solution* $(\tilde{u}, \tilde{v})$ *of the 1D model will be in* $C^m[0,1]$ *for all times and for* $\nu \geq 0$.

Proof. Differentiating the $\tilde{u}$ and $\tilde{v}$-equations w.r.t z, we get

$$(\tilde{u}_z)_t + 2\tilde{\psi}(\tilde{u}_z)_z - 2\tilde{v}\tilde{u}_z = -2\tilde{v}\tilde{u}_z - 2\tilde{u}\tilde{v}_z + \nu(\tilde{u}_z)_{zz},$$
$$(\tilde{v}_z)_t + 2\tilde{\psi}(\tilde{v}_z)_z - 2\tilde{v}\tilde{v}_z = 2\tilde{u}\tilde{u}_z - 2\tilde{v}\tilde{v}_z + \nu(\tilde{v}_z)_{zz}.$$

The convection term cancels one of the nonlinear terms.

$$(\tilde{u}_z^2)_t + 2\tilde{\psi}(\tilde{u}_z^2)_z = -4\tilde{u}\tilde{u}_z\tilde{v}_z + 2\nu\tilde{u}_z(\tilde{u}_z)_{zz}, \tag{8}$$
$$(\tilde{v}_z^2)_t + 2\tilde{\psi}(\tilde{v}_z^2)_z = 4\tilde{u}\tilde{u}_z\tilde{v}_z + 2\nu\tilde{v}_z(\tilde{v}_z)_{zz}. \tag{9}$$

Another cancelltion occurs, which gives rise to

$$\left(\tilde{u}_z^2 + \tilde{v}_z^2\right)_t + 2\tilde{\psi}\left(\tilde{u}_z^2 + \tilde{v}_z^2\right)_z = \nu\left(\tilde{u}_z^2 + \tilde{v}_z^2\right)_{zz} - 2\nu\left[(\tilde{u}_{zz})^2 + (\tilde{v}_{zz})^2\right].$$

Construction of a family of globally smooth solutions

Theorem 3. *Let $\phi(r)$ be a smooth cut-off function and u_1, ω_1 and ψ_1 be the solution of the 1D model. Define*

$$\begin{aligned} u^\theta(r,z,t) &= r u_1(z,t)\phi(r) + \tilde{u}(r,z,t), \\ \omega^\theta(r,z,t) &= r\omega_1(z,t)\phi(r) + \tilde{\omega}(r,z,t), \\ \psi^\theta(r,z,t) &= r\psi_1(z,t)\phi(r) + \tilde{\psi}(r,z,t). \end{aligned}$$

Then there exists a family of globally smooth functioons $\tilde{u}$, $\tilde{\omega}$ and $\tilde{\psi}$ such that u^θ, ω^θ and ψ^θ are globally smooth solutions of the 3D Navier-Stokes equations with finite energy.

A New 3D Model for NSE, [Hou-Lei, CPAM, 09]

Recall the reformulated 3D Navier-Stokes equations:

$$\begin{cases} \partial_t u_1 + u^r \partial_r u_1 + u^z \partial_z u_1 = \nu\big(\partial_r^2 + \frac{3}{r}\partial_r + \partial_z^2\big) u_1 + 2u_1\psi_{1z}, \\ \partial_t \omega_1 + u^r \partial_r \omega_1 + u^z \partial_z \omega_1 = \nu\big(\partial_r^2 + \frac{3}{r}\partial_r + \partial_z^2\big)\omega_1 + \big(u_1^2\big)_z, \\ -\big(\partial_r^2 + \frac{3}{r}\partial_r + \partial_z^2\big)\psi_1 = \omega_1, \end{cases} \tag{18}$$

where $u^r = -r\psi_{1z}$, $u^z = 2\psi_1 + r\psi_{1r}$. Our 3D model is derived by simply dropping the convective term from (18):

$$\begin{cases} \partial_t u_1 = \nu\big(\partial_r^2 + \frac{3}{r}\partial_r + \partial_z^2\big) u_1 + 2u_1\psi_{1z}, \\ \partial_t \omega_1 = \nu\big(\partial_r^2 + \frac{3}{r}\partial_r + \partial_z^2\big)\omega_1 + (u_1^2)_z, \\ -\big(\partial_r^2 + \frac{3}{r}\partial_r + \partial_z^2\big)\psi_1 = \omega_1. \end{cases} \tag{19}$$

Note that (19) is already a closed system, and $u_1 = u^\theta/r$ characterizes the axial vorticity near $r = 0$.

Properties of the 3D Model [Hou-Lei, CPAM, 09]

This 3D model shares many important properties with the axisymmetric Navier-Stokes equations.

First of all, one can define an incompressible velocity field in the model equations (19).

$$\mathbf{u}(t,x) = u^r(t,r,z)e_r + u^\theta(t,r,z)e_\theta + u^z(t,r,z)e_z, \tag{20}$$

$$u^\theta = ru_1,\ u^r = -r\psi_{1z}, \quad u^z = 2\psi_1 + r\psi_{1r}, \tag{21}$$

where $x = (x_1,\ x_2,\ z)$, $r = \sqrt{x_1^2 + x_2^2}$. It is easy to check that

$$\nabla \cdot \mathbf{u} = \partial_r u^r + \partial_z u^z + \frac{u^r}{r} = 0, \tag{22}$$

which is the same as the Navier-Stokes equations.

Properties of the 3D Model–continued

Our model enjoys the following properties ([Hou-Lei, CPAM-09]):

Theorem 5. Energy identity. The smooth solution of (19) satisfies

$$\frac{1}{2}\frac{d}{dt}\int \left(|u_1|^2 + 2|D\psi_1|^2\right) r^3 dr dz + \nu \int \left(|Du_1|^2 + 2|D^2\psi_1|^2\right) r^3 dr dz = 0,$$

which has been proved to be equivalent to that of the Navier-Stokes equations. Here D is the first order derivative operator defined in $\mathbb{R}^5$.

Theorem 6. A non-blowup criterion of Beale-Kato-Majda type. A smooth solution (u_1, ω_1, ψ_1) of the model (19) for $0 \le t < T$ blows up at time $t = T$ if and only if

$$\int_0^T \|\nabla \times \mathbf{u}\|_{\mathrm{BMO}(\mathbb{R}^3)} dt = \infty,$$

where $\mathbf{u}$ is defined in (20)-(21).

Properties of the 3D Model–continued

Theorem 7. A non-blowup criterion of Prodi-Serrin type. A weak solution (u_1, ω_1, ψ_1) of the model (19) is smooth on $[0, T] \times \mathbb{R}^3$ provided that

$$\|u^\theta\|_{L_t^q L_x^p([0,T]\times\mathbb{R}^3)} < \infty \tag{23}$$

for some p, q satisfying $\frac{3}{p} + \frac{2}{q} \leq 1$ with $3 < p \leq \infty$ and $2 \leq q < \infty$.

Theorem 8. An analog of Caffarelli-Kohn-Nirenberg partial regularity result [Hou-Lei, CMP-09]. For any suitable weak solution of the 3D model equations (19) on an open set in space-time, the one-dimensional Hausdorff measure of the associated singular set is zero.

Numerical evidence for a potential finite time singularity

Innitial condition we consider in our numerical computations is given by

$$\begin{aligned} u_1(z,r,0) &= (1+\sin(4\pi z))(r^2-1)^{20}(r^2-1.2)^{30}, \quad 0 \le r \le 1, \\ \psi_1(z,r,0) &= 0, \\ \omega_1(z,r,0) &= 0. \end{aligned}$$

A second order finite difference discretization is used in space, and the classical fourth order Runge-Kutta method is used to discretize in time. We use the following coordinate transformation along the r-direction to achieve the adaptivity:

$$r = f(\alpha) \equiv \alpha - 0.9\sin(\pi\alpha)/\pi.$$

We use an effective resolution up to 4096^3 for the 3D problem.

A 3D view of u_1 at $t = 0.02$.

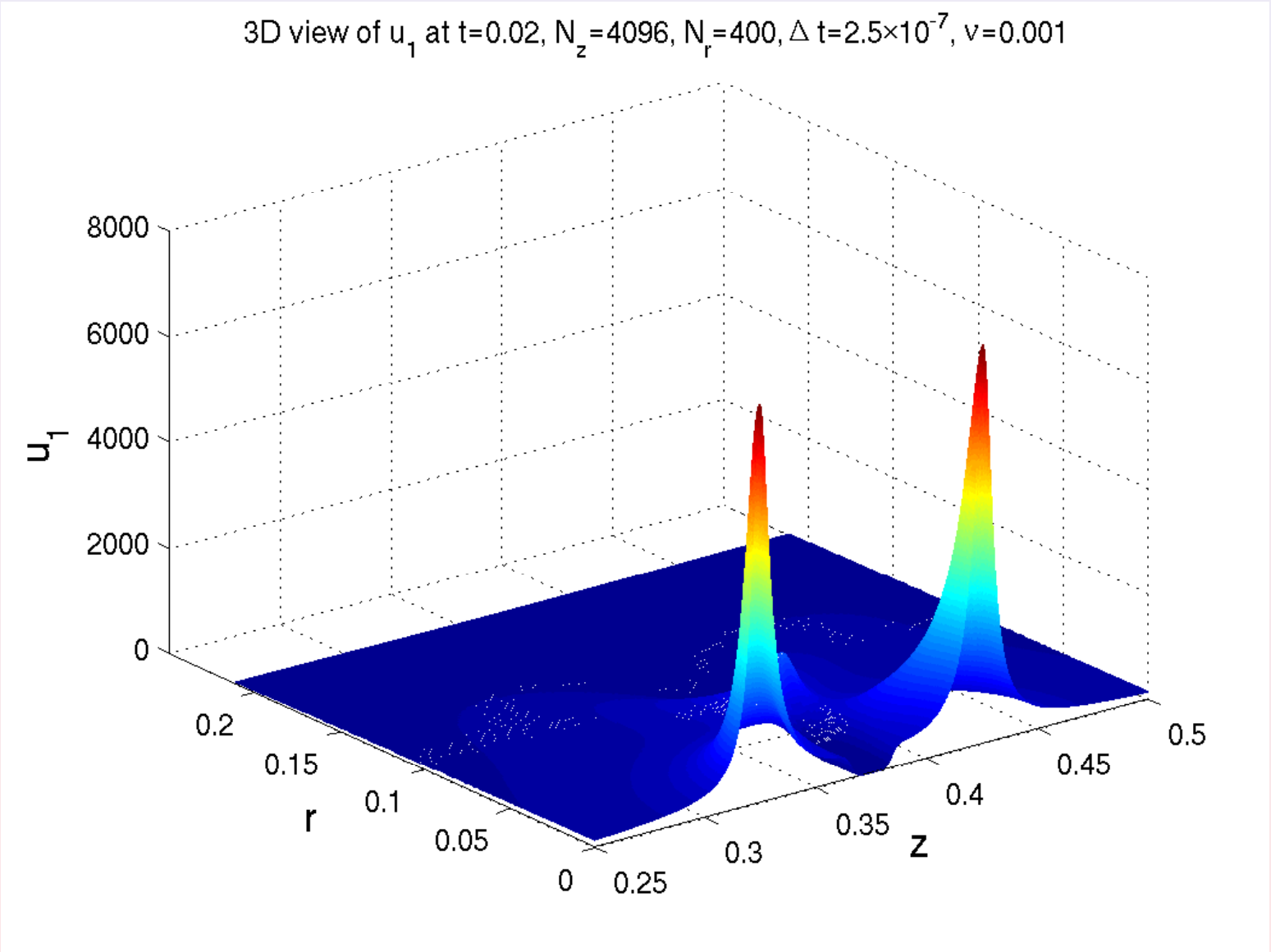

A 3D view of u_1 at $t = 0.021$.

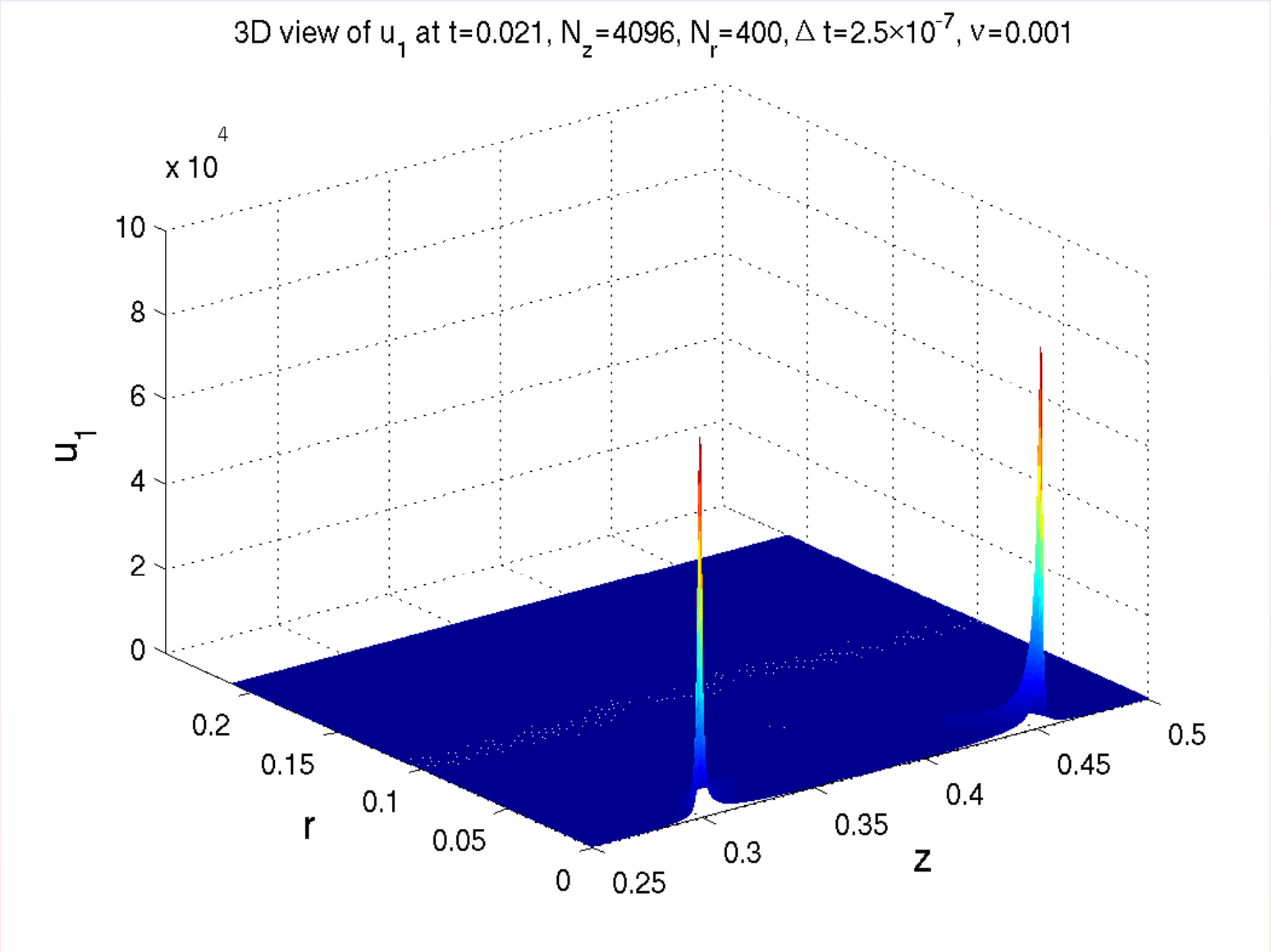

Asymptotic blowup fit: $\|u_1\|_\infty^{-1} \approx \frac{(T-t)}{C}$, with limiting values $T = 0.021083$ and $C = 8.1901$.

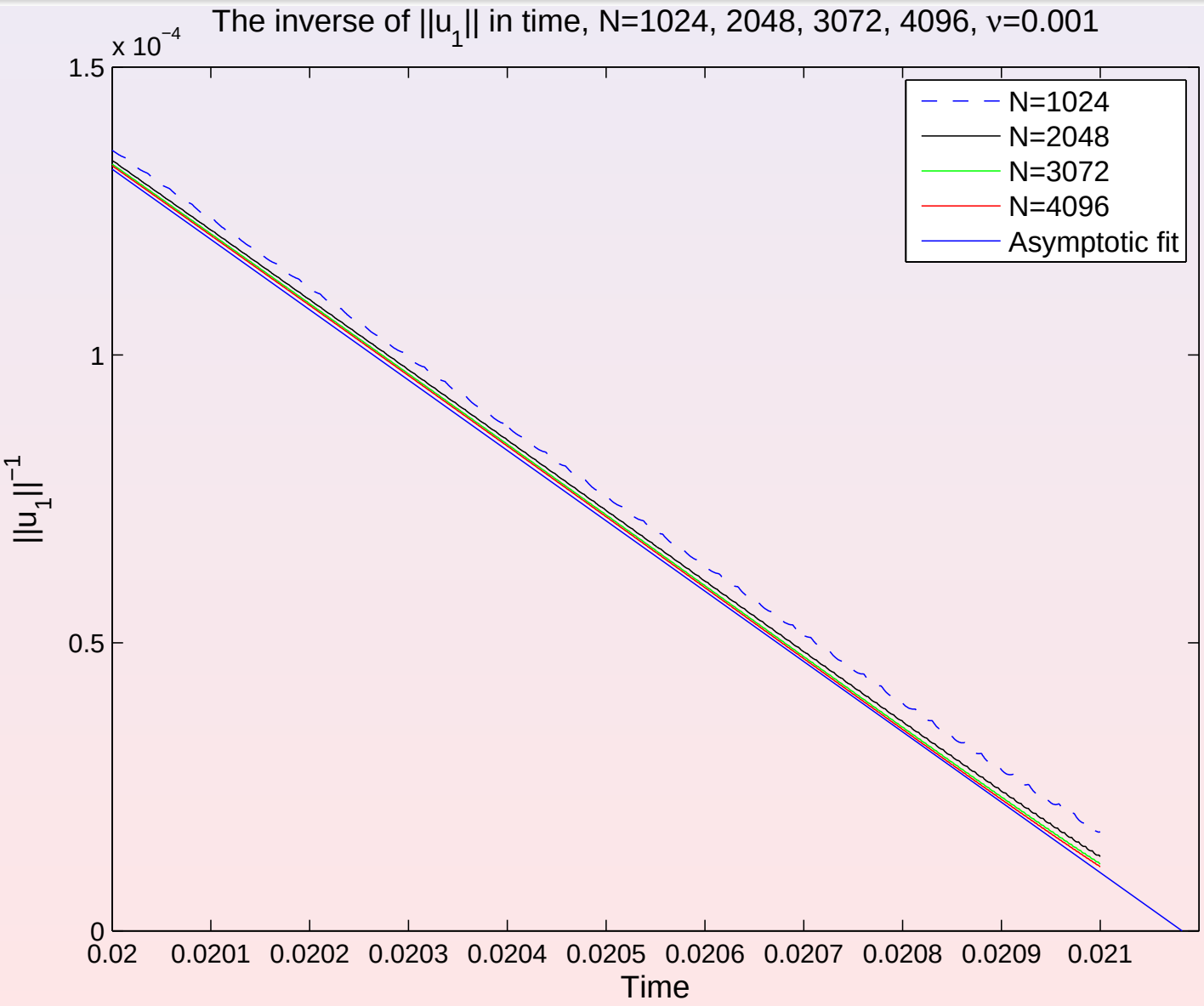

Asymptotic blowup rate: $\|u_1\|_\infty \approx \frac{C}{(T-t)}$, with $T = 0.02109$ and $C = 8.20348$.

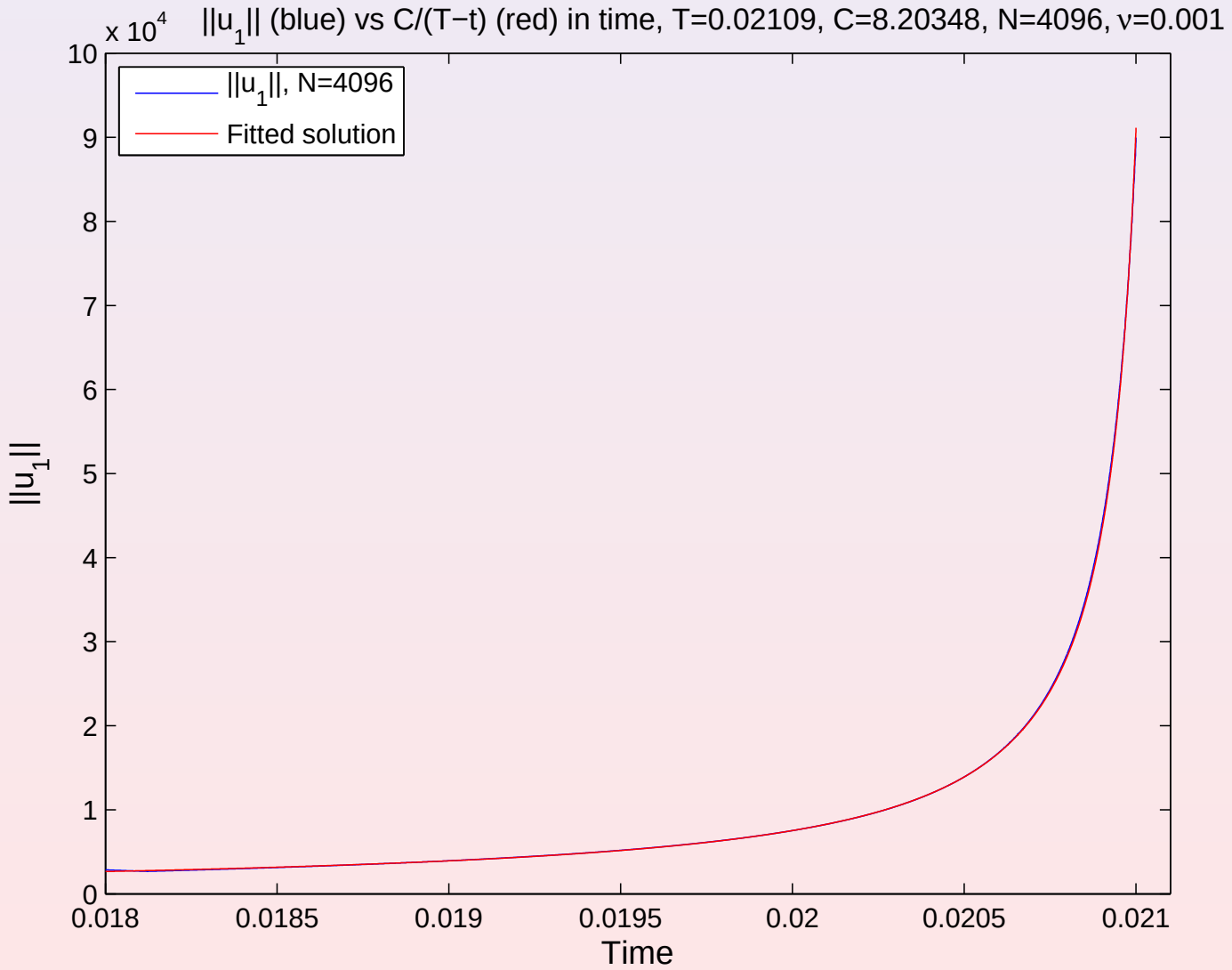

Local alignment of u_1 and ψ_{1z} at $t = 0.02$. Recall $(u_1)_t = 2u_1\psi_{1z} + \nu\Delta u_1,\ (\omega_1)_t = (u_1^2)_z + \nu\Delta\omega_1$.

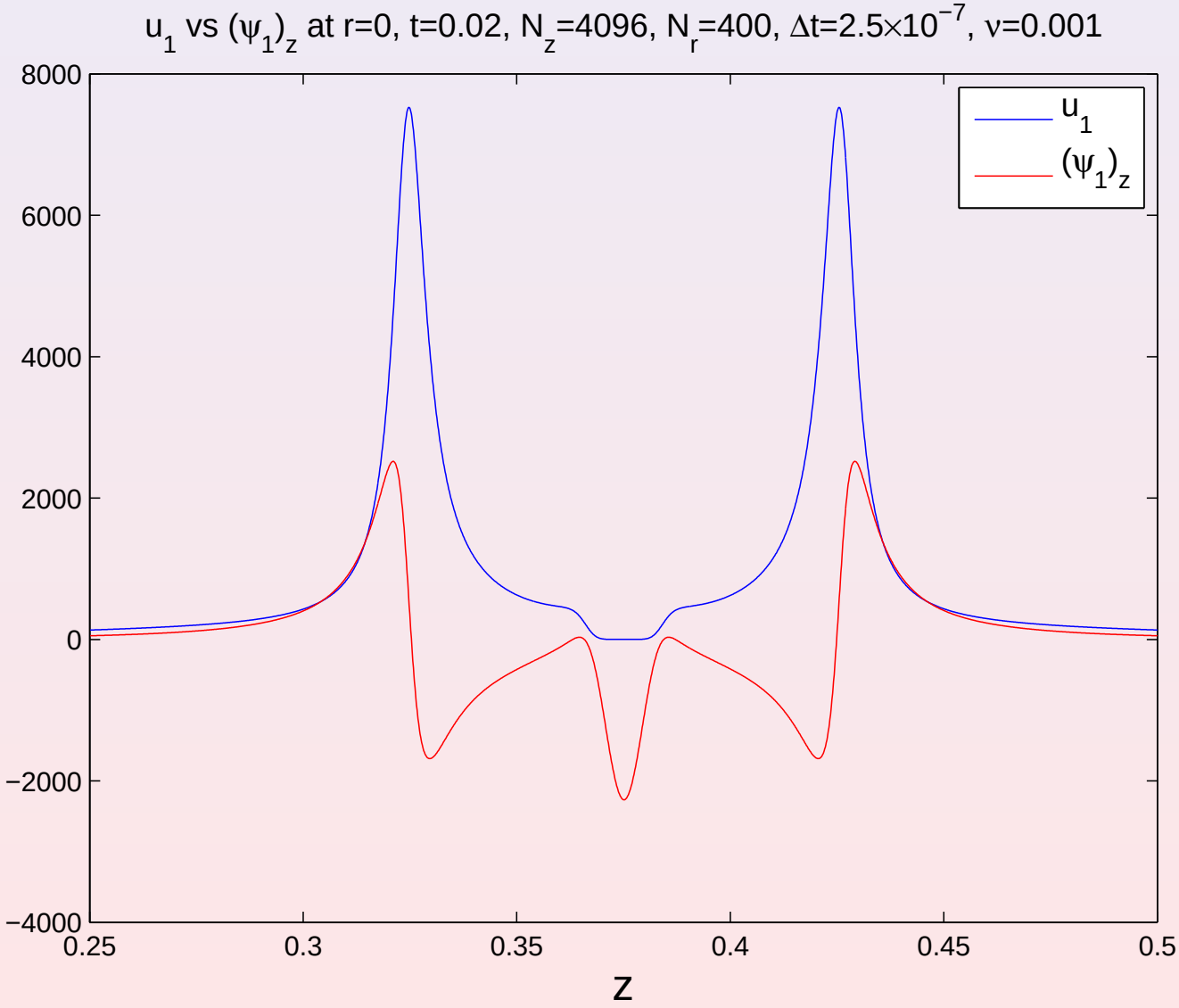

Local alignment of u_1 and ψ_{1z} at $t = 0.021$.

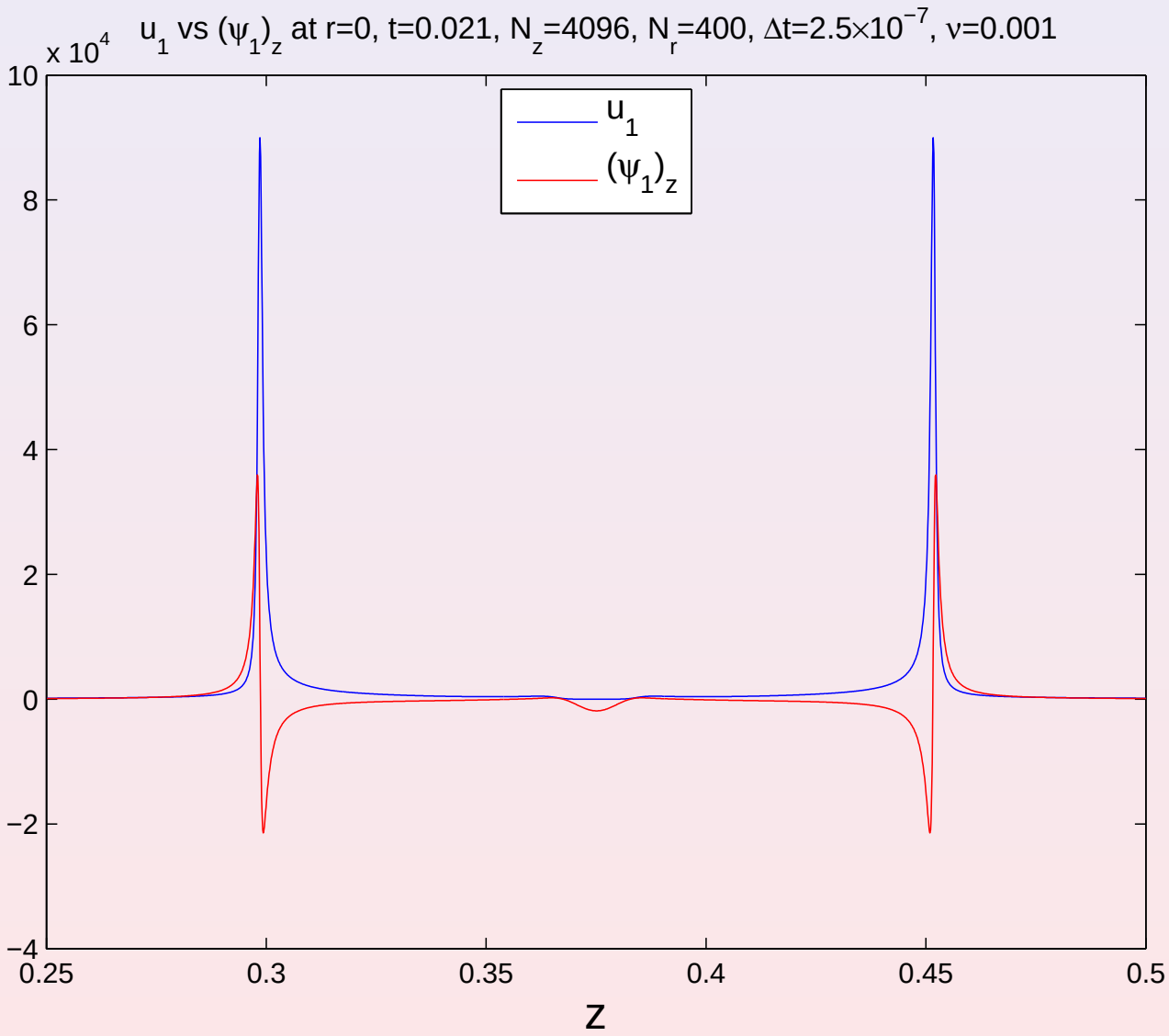

The effect of convection.

To study the effect of convection, we add the convection term back to the 3D model and solve the Navier-Stokes equations using the solution of the 3D model at $t = 0.02$ as the initial condition.

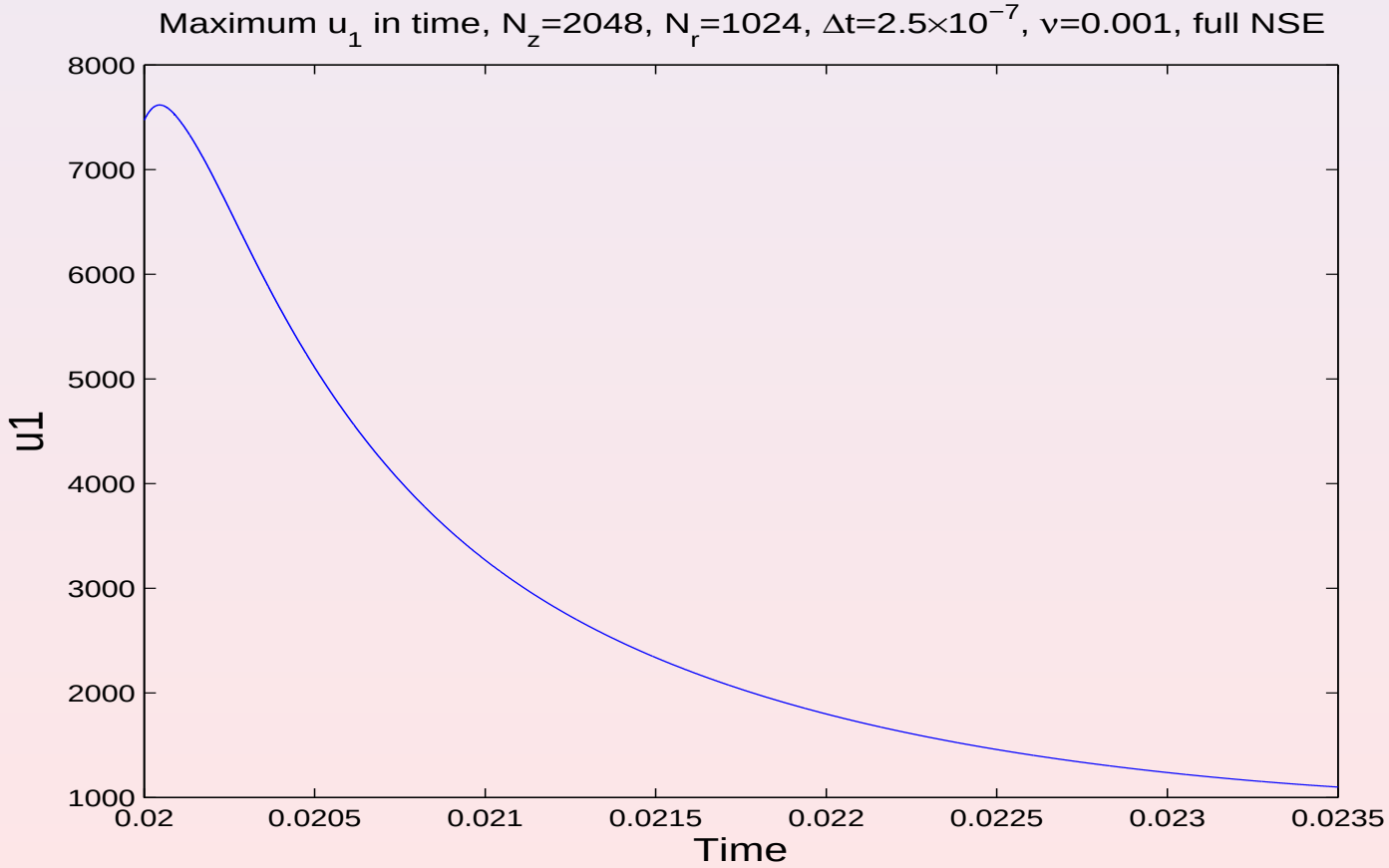

Contours of initial data for u_1.

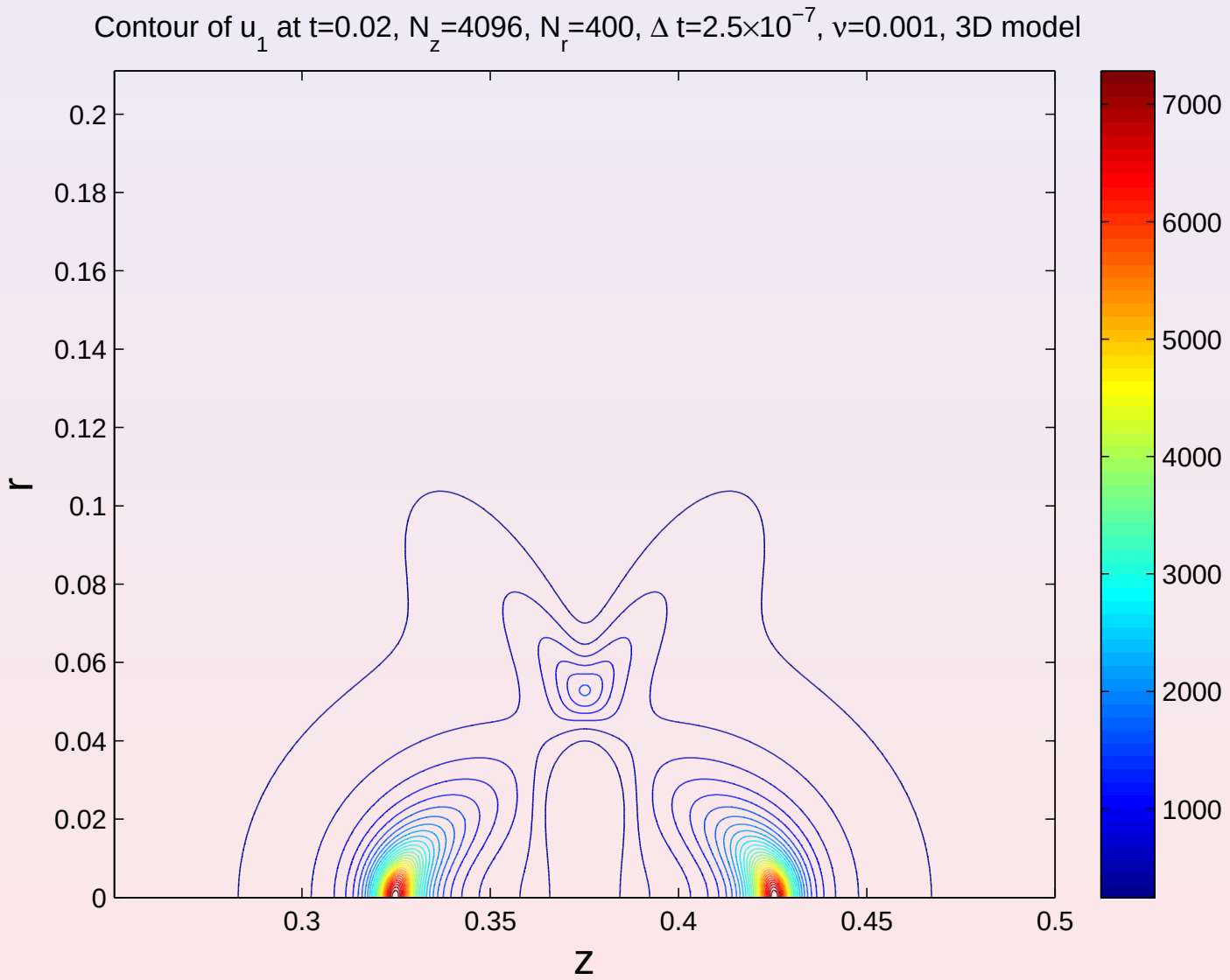

Contours of u_1 at $t = 0.021$, solution of full NSE.

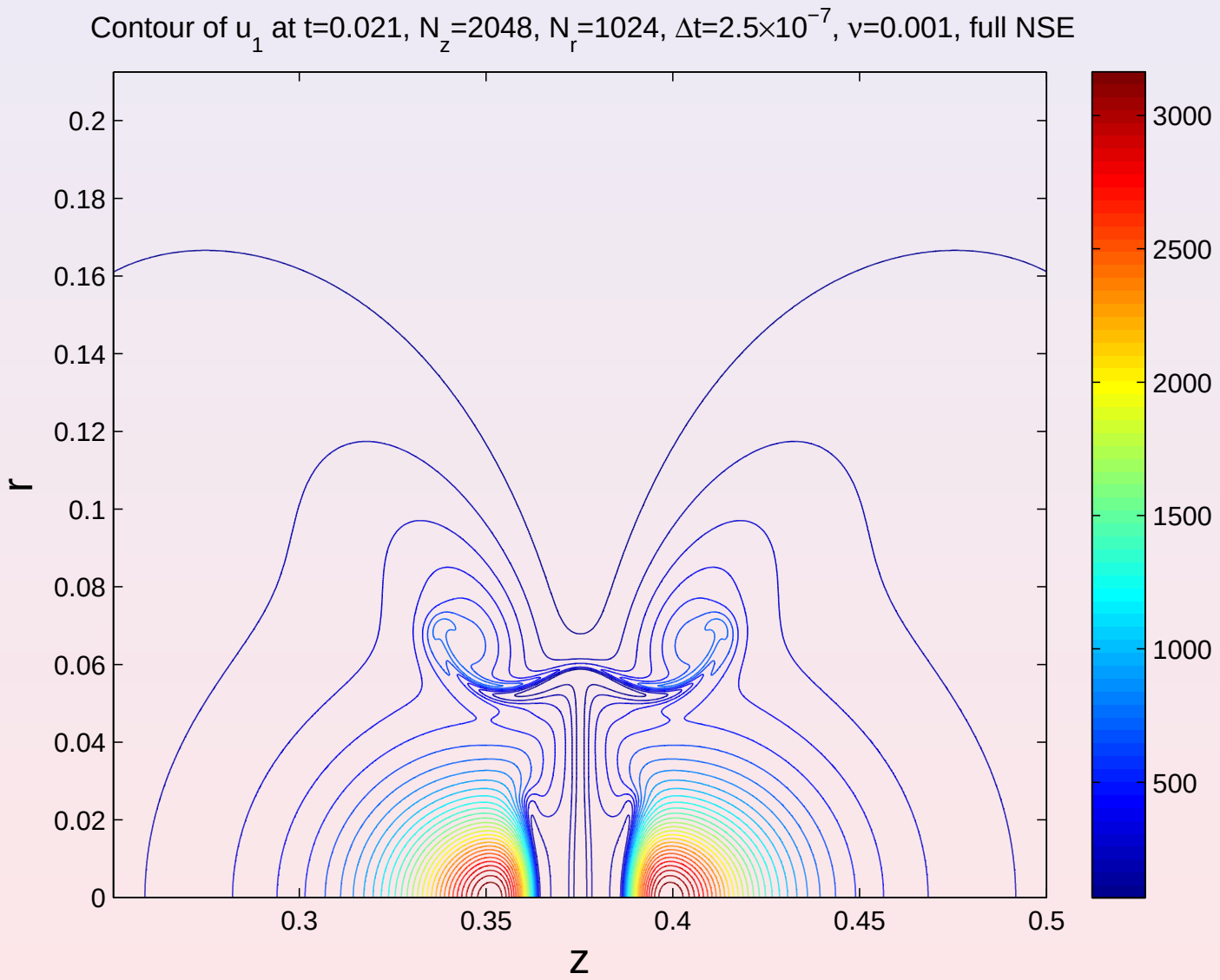

Contours of u_1 at $t = 0.0235$, solution of full NSE.

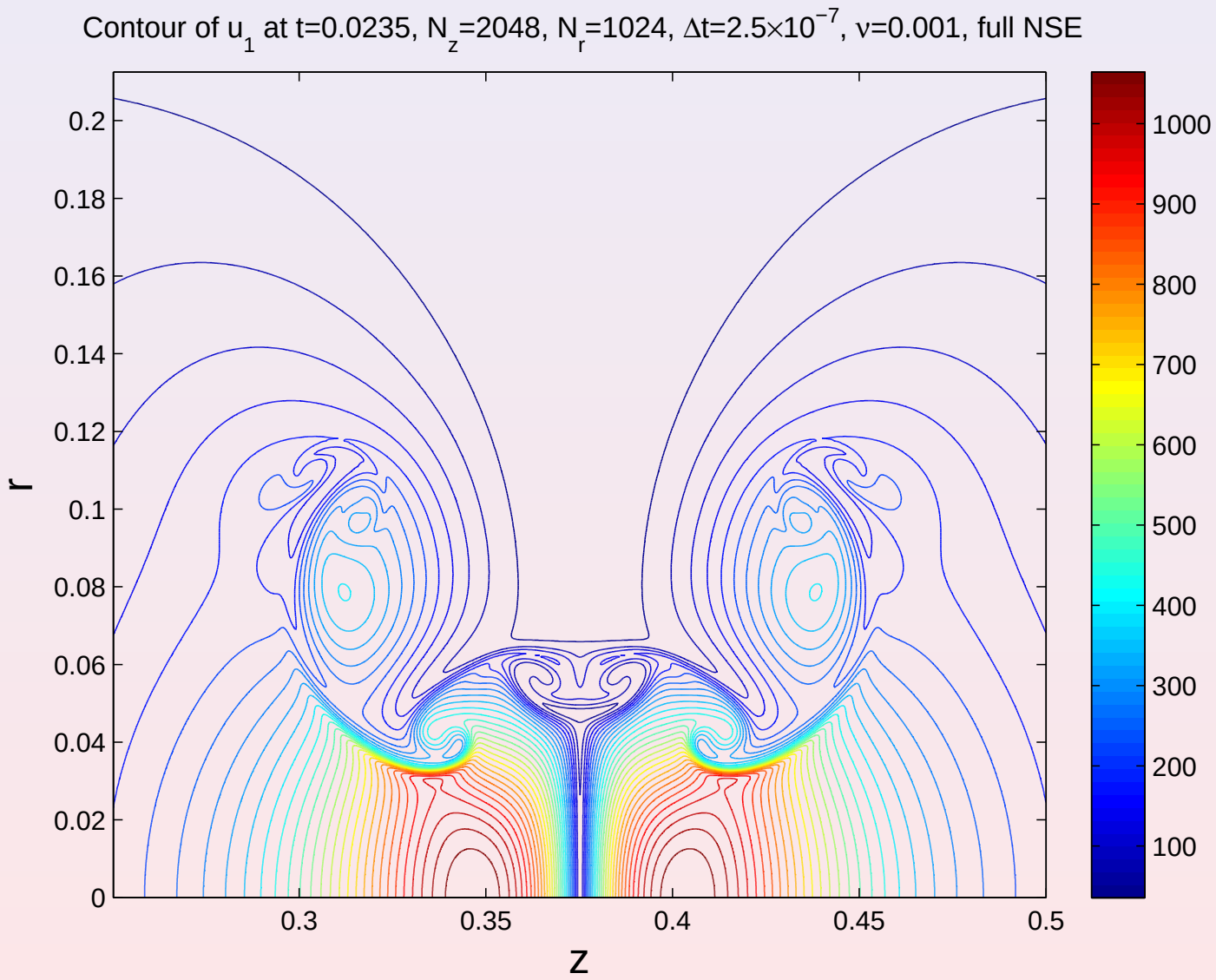

Recent theortical progress for the 3D model

Theorem 9. [Hou-Shi-Wang, 12]. Consider the 3D inviscid model

$$\begin{cases} u_t = 2u\psi_z, \quad \omega_t = (u^2)_z, \\ -(\partial_x^2 + \partial_y^2 + \partial_z^2)\psi = \omega, \quad 0 \le x,\ y,\ z \le 1, \end{cases} \tag{24}$$

with boundary condition $\psi = 0$ at $x = 0,\ 1,\ y = 0,\ 1,\ z = 1$, and $(\alpha \frac{\partial \psi}{\partial z} + \psi)|_{z=0} = 0$ for some $0 < \alpha < 1$. If the initial conditions, u_0 and ψ_0, are smooth, satisfying $u_0 = 0$ at $z = 0,\ 1$, and

$$\int_{[0,1]^3} \log(u_0)\phi(x,y,z)dxdydz \ge 0, \quad \int_{[0,1]^3} (\psi_0)_z \phi(x,y,z)dxdydz > 0,$$

where $\phi(x,y,z) = \sin(x)\sin(y)\cosh(\alpha(1-z))$, then the 3D inviscid model must develop a finite time singularity. Moreover, if the ω-equation is viscous and ω satisfies the same boundary condition as ψ, then the 3D model with partial viscosity must develop a finite time singularity.

Global regularity for a class of initial-boundary data

Let $v = \psi_z$, we can rewrite the 3D model as follows:

$$\begin{cases} u_t &= 2uv \\ -\Delta v_t &= (u^2)_{zz} \end{cases}, \quad (x,z) \in \Omega = [0,\delta]^3. \tag{25}$$

The initial and boundary conditions are given as follows:

$$v|_{\partial\Omega} = -4, \ v(x,y,z,0) = v_0(x,y,z), \ u(x,y,z,0) = u_0(x,y,z). \tag{26}$$

Theorem 10. Assume $u_0^2, \ v_0 \in H^m(\Omega)$ for $m \geq 2$ and $v_0 \leq -4$ for $x \in \Omega$, then the solution of the 3D model remains smooth for all times as long as the following holds

$$\max(4C_m, 1)\left(\|v_0\|_{H^m} + C_m\|u_0^2\|_{H^m}\right)\delta < 1, \tag{27}$$

where C_m is a Sobolev interpolation constant.

Potential singularity for 3D Euler equation

- Inspired by the previous study, we discover a class of initial data that lead to potentially singular solutions of 3D Euler equations.
- Main features of our study:
  - the singularity occurs at a stagnation point where the effect of convection is minimized.
  - strong symmetry (axisymmetry plus odd/even symmetry in z)
  - devises highly effective algorithms for adequate resolution
  - employs rigorous criteria for confirmation of singularity

Vorticity Kinematics

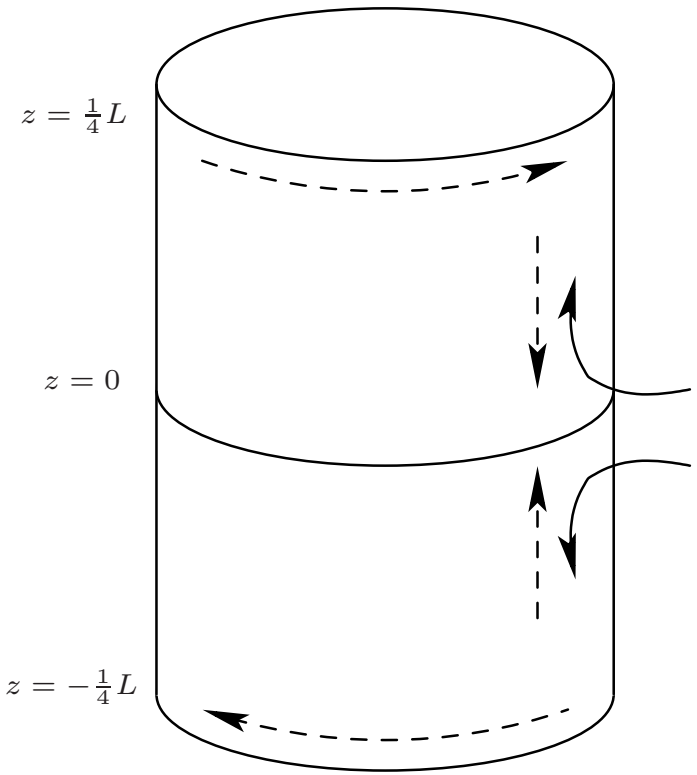

Figure : Vorticity kinematics of the 3D Euler singularity; solid: vortex lines; straight dashed lines: axial flow; curved dash lines: vortical circulation.

Local Flow Field

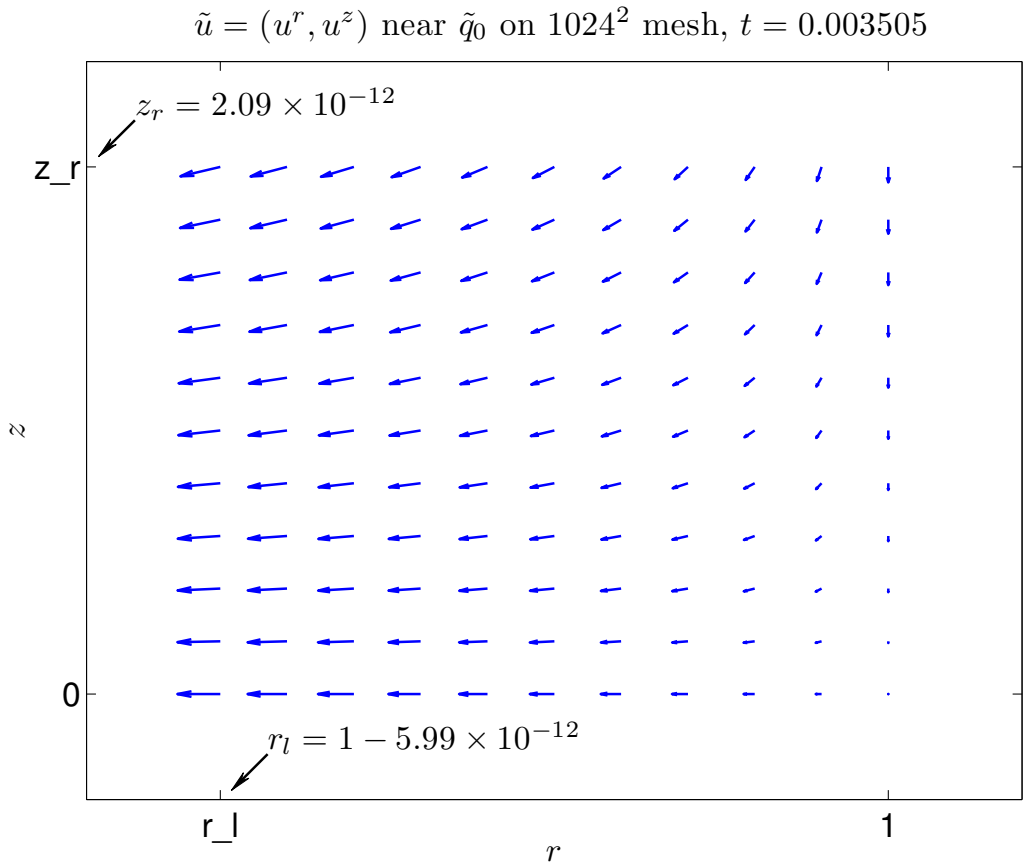

Figure : The 2D flow field $\tilde{u} = (u^r, u^z)^T$ near the maximum vorticity.

Outline

3D Axisymmetric Euler Equations

- Equations being solved: the 3D axisymmetric Euler (Hou-Li, 2008)

$$u_{1,t} + u^r u_{1,r} + u^z u_{1,z} = 2u_1\psi_{1,z},$$
$$\omega_{1,t} + u^r \omega_{1,r} + u^z \omega_{1,z} = (u_1^2)_z,$$
$$-\left[\partial_r^2 + \tfrac{3}{r}\partial_r + \partial_z^2\right]\psi_1 = \omega_1,$$

where $u_1 = u^\theta/r,\ \omega_1 = \omega^\theta/r,\ \psi_1 = \psi^\theta/r$.

  - $u^r = -r\psi_{1,z},\ u^z = 2\psi_1 + r\psi_{1,r}$: the radial/axial velocity components.
  - Initial condition:
    $u_1(r,z,0) = 100e^{-30(1-r^2)^4}\sin\left(\frac{2\pi z}{L}\right), \quad \omega_1(r,z,0) = \psi_1(r,z,0) = 0.$
  - No flow boundary condition $\psi_1 = 0$ at $r = 1$ and periodic BC in z.

Outline of the Method

- Discretization in space: a hybrid 6th-order Galerkin and 6th-order finite difference method, on an adaptive (moving) mesh that is dynamically adjusted to the evolving solution
- Discretization in time: an explicit 4th-order Runge-Kutta method, with an adaptively chosen time step
- Solution advanced indefinitely in time until either
  - the time step drops below 10^{-12}, or
  - the minimum mesh spacing in r drops below $\epsilon_r = 10^{-15}$, or
  - the minimum mesh spacing in z drops below $\epsilon_z = 10^{-15} L$,

  whichever happens first

Outline

Adaptive Methods for Singularity Detection

Existing methods for computing (self-similar) singularities:

- dynamic rescaling (McLaughlin et al. 1986: nonlinear Schrödinger)
- adaptive mesh refinement (Berger and Kohn 1988: semilinear heat)
- moving mesh method (Budd et al. 1996: semilinear heat; Budd et al. 1999: nonlinear Schrödinger)

- However, these methods require knowledge of the singularity
- discrete approximation of mesh mapping functions can result in significant loss of accuracy

Our Approach: Defining the Adaptive Mesh

- We observe that vorticity tends to concentrate at a single point in the *rz*-plane.
- This motivates the development of the following special mesh adaptation strategy.
- The adaptive mesh covering the computational domain is constructed from a pair of analytic mesh mapping functions:

$$r = r(\rho), \qquad z = z(\eta),$$

where each mesh mapping function contains a small number of parameters, which are dynamically adjusted so that along each dimension a certain fraction (e.g. 50%) of the mesh points is placed in a small neighborhood of the singularity

Advancing the Solution

- The Poisson equation for ψ_1 is solved in the $\rho\eta$-space using a 6th order B-spline based Galerkin method.
- The evolutionary equations for u_1 and ω_1 are semi-discretized in the $\rho\eta$-space, where
  - the space derivatives are expressed in the $\rho\eta$-coordinates and are approximated using 6th-order centered difference scheme, e.g.

$$v_{r,ij} = \frac{v_{\rho,ij}}{r_{\rho,j}} \approx \frac{1}{r_{\rho,j}} (D^6_{\rho,0} v_i)_j$$

  - the resulting system of ODEs is integrated in time using an explicit 4th-order Runge-Kutta method

Outline

Effectiveness of the Adaptive Mesh

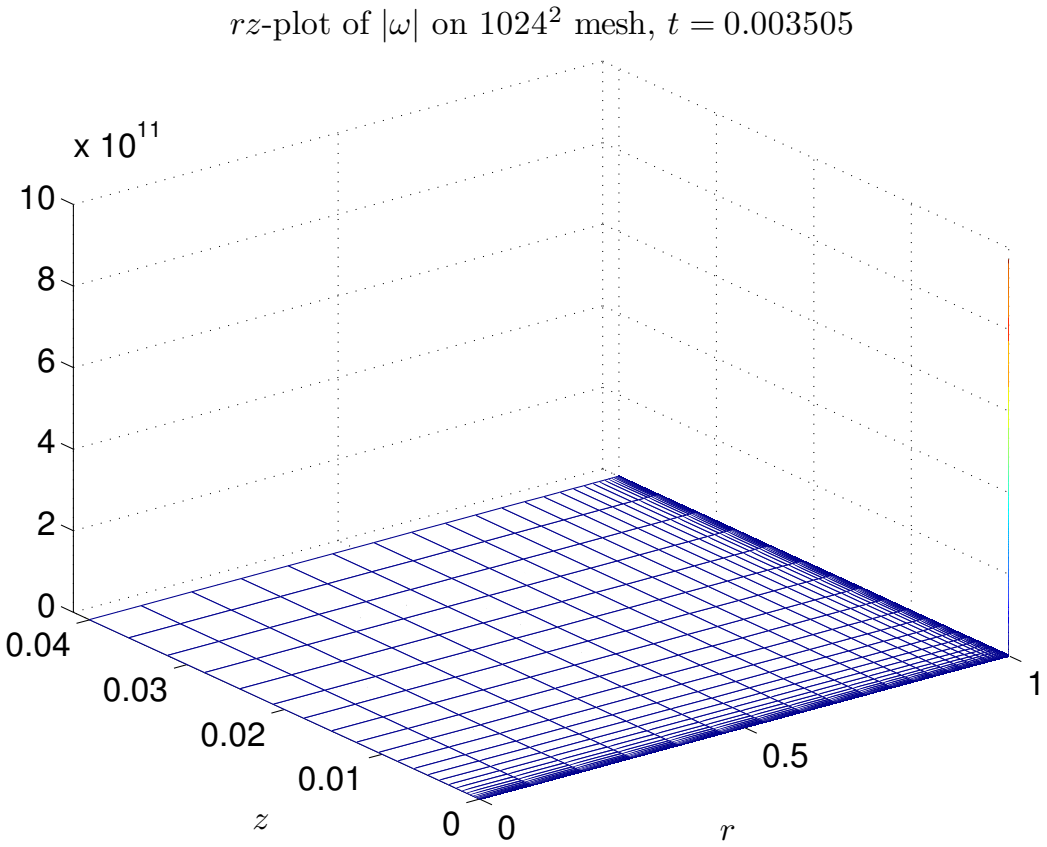

Figure : The vorticity function $|\omega|$ on the 1024×1024 mesh at $t = 0.003505$; plot shown in *rz*-coordinates with $1 : 10$ sub-sampling in each dimension.

Effectiveness of the Adaptive Mesh (Cont'd)

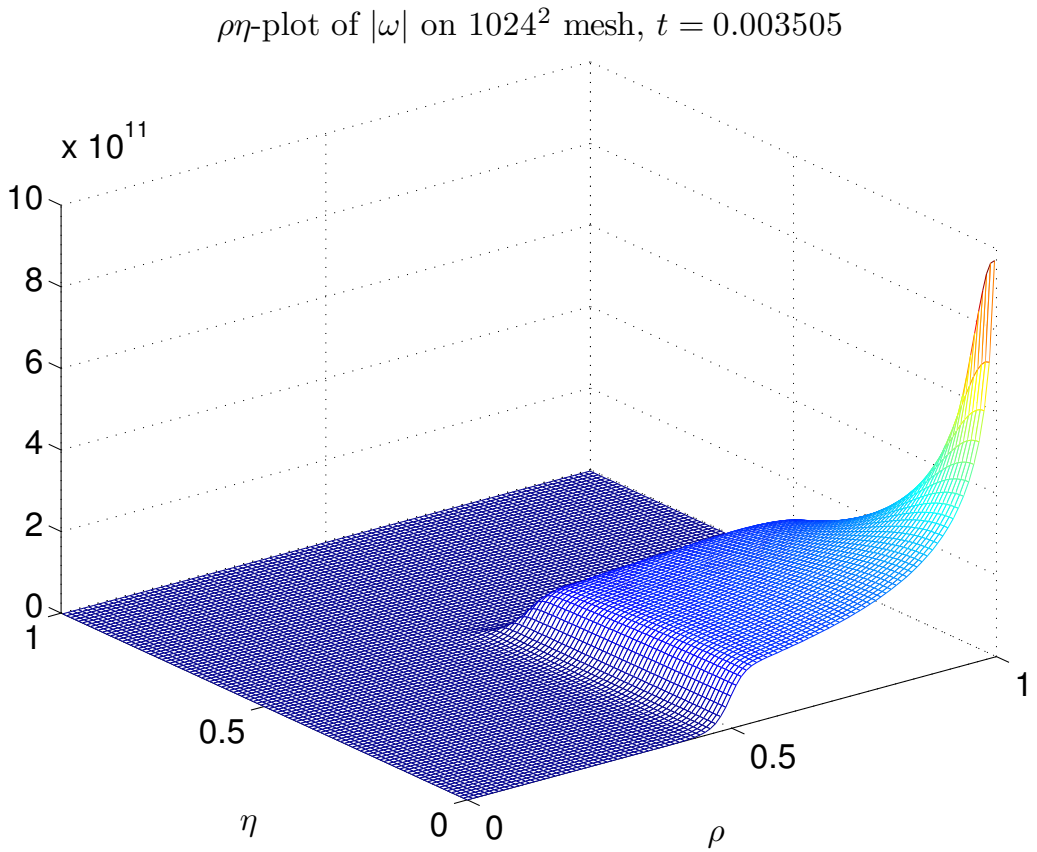

Figure : The vorticity function $|\omega|$ on the 1024×1024 mesh at $t = 0.003505$; plot shown in $\rho\eta$-coordinates with $1 : 10$ sub-sampling in each dimension.

Effective Mesh Resolutions

Table : Effective mesh resolutions M_∞, N_∞ near the maximum vorticity at selected time t.

Mesh size	$t = 0.003505$	
	M_∞	N_∞
1024×1024	1.9923×10^{12}	1.6708×10^{12}
1280×1280	2.4999×10^{12}	2.0844×10^{12}
1536×1536	2.9866×10^{12}	2.5079×10^{12}
1792×1792	3.4951×10^{12}	2.9288×10^{12}
2048×2048	3.9942×10^{12}	3.3444×10^{12}

Backward Error Analysis of the Linear Solve

Table : Backward errors of the linear solve $Ax = b$ associated with the elliptic equation for ψ_1 at $t = 0.003505$.

Mesh size	$t = 0.003505$				
	ω_1	κ_{ω_1}	ω_2	κ_{ω_2}	$\|\delta x\|_\infty / \|x\|_\infty$
512	5.9×10^{-15}	1247.3	1.9×10^{-23}	2.3×10^{7}	7.3×10^{-12}
768	1.1×10^{-15}	1788.84	2.1×10^{-23}	5.2×10^{7}	1.9×10^{-12}
1024	1.5×10^{-15}	6748.83	6.4×10^{-23}	9.3×10^{7}	9.9×10^{-12}

The linear system is solved using a parallel sparse direct solver called PaStiX package. Here ω_1, ω_2 are the componentwise backward errors of first and second kind, and κ_{ω_1}, κ_{ω_2} are the componentwise condition numbers of first and second kind. It can be shown that (Arioli 1989)

$$\frac{\|\delta x\|_\infty}{\|x\|_\infty} \leq \omega_1 \kappa_{\omega_1} + \omega_2 \kappa_{\omega_2}.$$

Outline

Maximum Vorticity

Table : Maximum vorticity $\|\omega\|_\infty = \|\nabla \times u\|_\infty$ at selected time t.

Mesh size	$\|\omega\|_\infty$		
	$t = 0$	$t = 0.0034$	$t = 0.003505$
1024×1024	3.7699×10^3	4.3127×10^6	1.2416×10^{12}
1280×1280	3.7699×10^3	4.3127×10^6	1.2407×10^{12}
1536×1536	3.7699×10^3	4.3127×10^6	1.2403×10^{12}
1792×1792	3.7699×10^3	4.3127×10^6	1.2401×10^{12}
2048×2048	3.7699×10^3	4.3127×10^6	1.2401×10^{12}

Maximum Vorticity (Cont'd)

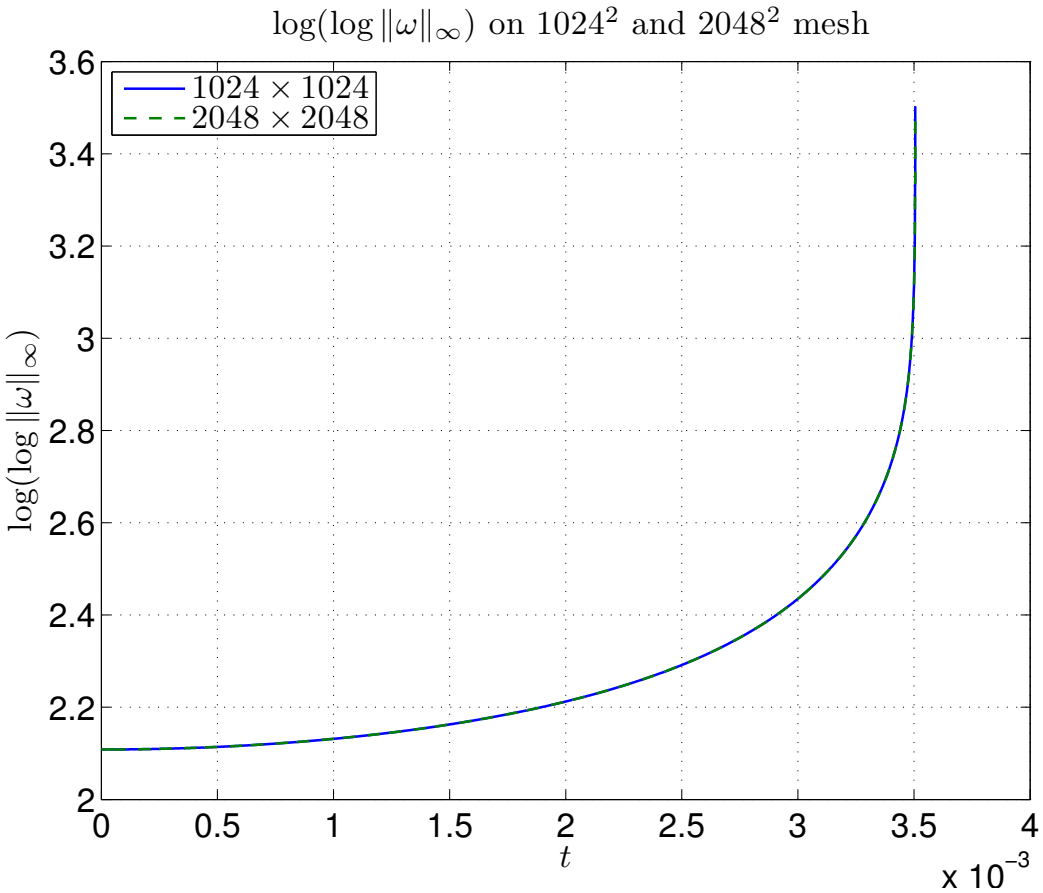

Figure : The double logarithm of the maximum vorticity, $\log(\log\|\omega\|_\infty)$, computed on the 1024×1024 and the 2048×2048 mesh.

Resolution Study on Primitive Variables

Table : Sup-norm relative error and numerical order of convergence of the transformed primitive variables u_1 at selected time t.

Mesh size	$t = 0.003505$	
	Error	Order
1024×1024	9.4615×10^{-6}	–
1280×1280	3.6556×10^{-6}	4.2618
1536×1536	1.5939×10^{-6}	4.5526
1792×1792	7.5561×10^{-7}	4.8423
Sup-norm	1.0000×10^{2}	–

Resolution Study on Primitive Variables (Cont'd)

Table : Sup-norm relative error and numerical order of convergence of the transformed primitive variables ω_1 at selected time t.

Mesh size	$t = 0.003505$	
	Error	Order
1024×1024	6.4354×10^{-4}	–
1280×1280	2.4201×10^{-4}	4.3829
1536×1536	1.1800×10^{-4}	3.9396
1792×1792	6.4388×10^{-5}	3.9297
Sup-norm	1.0877×10^{6}	–

Resolution Study on Primitive Variables (Cont'd)

Table : Sup-norm relative error and numerical order of convergence of the transformed primitive variables ψ_1 at selected time t.

Mesh size	$t = 0.003505$	
	Error	Order
1024×1024	2.8180×10^{-10}	–
1280×1280	4.7546×10^{-11}	7.9746
1536×1536	1.0873×10^{-11}	8.0925
1792×1792	2.9518×10^{-12}	8.4583
Sup-norm	2.1610×10^{-1}	–

Resolution Study on Conserved Quantities

Table : Kinetic energy E, minimum circulation Γ_1, maximum circulation Γ_2 and their maximum (relative) change over $[0, 0.003505]$.

Mesh size	$t = 0.003505$		
	$\|\delta E\|_{\infty,t}$	$\|\delta\Gamma_1\|_{\infty,t}$	$\|\delta\Gamma_2\|_{\infty,t}$
1024×1024	1.53×10^{-11}	4.35×10^{-17}	1.25×10^{-14}
1280×1280	4.17×10^{-12}	3.30×10^{-17}	7.78×10^{-15}
1536×1536	2.08×10^{-12}	3.13×10^{-17}	9.95×10^{-15}
1792×1792	6.47×10^{-13}	2.77×10^{-17}	2.14×10^{-14}
2048×2048	6.66×10^{-13}	2.53×10^{-17}	3.49×10^{-14}
Init. value	55.93	0.00	628.32

Outline

The Beale-Kato-Majda (BKM) Criterion

- The main tool for studying blowup/non-blowup: the Beale-Kato-Majda (BKM) criterion (Beale et al. 1984)

Theorem

Let u be a solution of the 3D Euler equations, and suppose there is a time t_s such that the solution cannot be continued in the class

$$u \in C([0,t];H^m) \cap C^1([0,t];H^{m-1}), \qquad m \geq 3$$

to $t = t_s$. Assume that t_s is the first such time. Then

$$\int_0^{t_s} \|\omega(\cdot,t)\|_\infty \, dt = \infty, \qquad \omega = \nabla \times u.$$

Applying the BKM Criterion

- The "standard" approach to singularity detection:
  1. assume the existence of an inverse power-law

$$\|\omega(\cdot,t)\|_\infty \sim c(t_s - t)^{-\gamma}, \qquad c,\ \gamma > 0$$

  2. estimate t_s and γ using a line fitting:

$$\left[\frac{d}{dt}\log\|\omega(\cdot,t)\|_\infty\right]^{-1} \sim \frac{1}{\gamma}(t_s - t)$$

  3. estimate c using another line fitting:

$$\log\|\omega(\cdot,t)\|_\infty \sim -\gamma\log(\hat{t}_s - t) + \log c,$$

  where $\hat{t}_s$ is the singularity time estimated in step 2

Our Criteria

- Our criteria for choosing the fitting interval $[\tau_1, \tau_2]$:
  - τ_2 is the last time at which the solution is still "accurate"
  - choose the fitting interval $[\tau_1, \tau_2]$ in the asymptotic regime.
- Our criteria for a successful line fitting:
  - both τ_2 and the line-fitting predicted singularity time $\hat{t}_s$ converge to the same finite value as the mesh is refined; the convergence should be monotone, i.e. $\tau_2 \uparrow t_s$, $\hat{t}_s \downarrow t_s$
  - τ_1 converges to a finite value that is strictly less than t_s as the mesh is refined

Applying the Ideas: Computing the Line Fitting

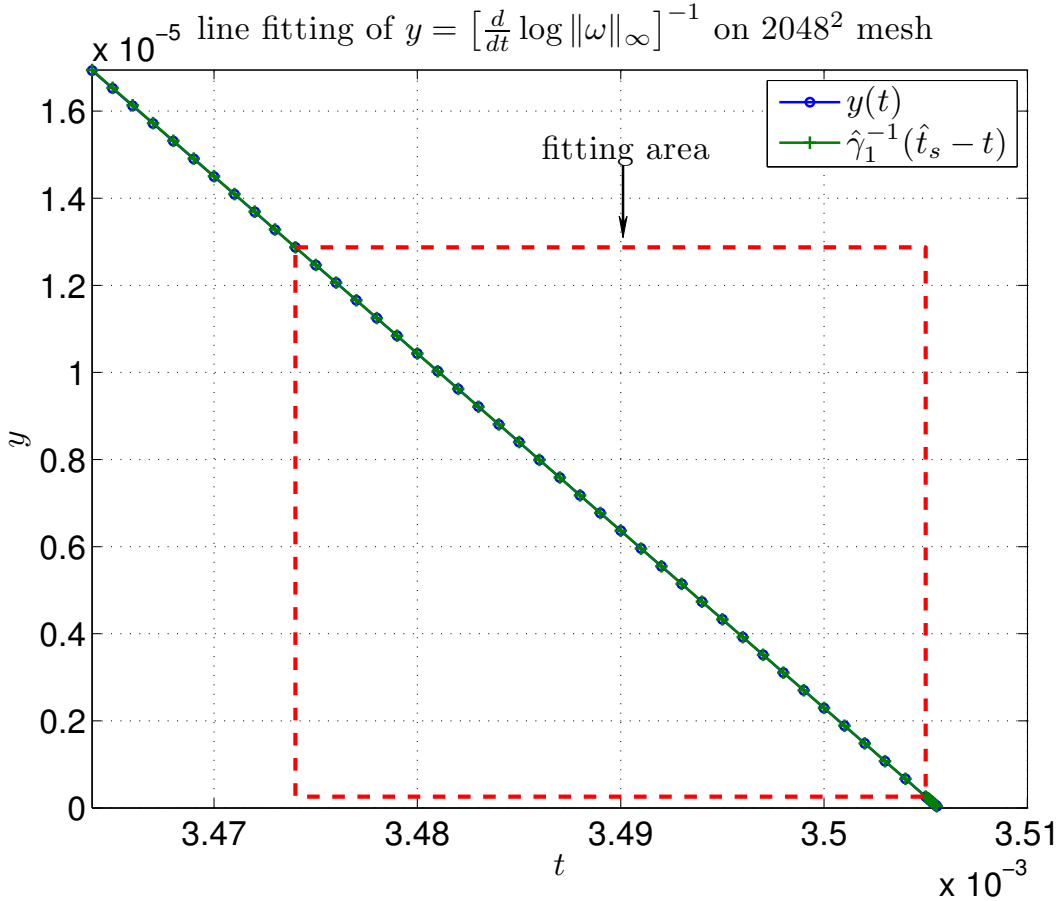

Figure : Inverse logarithmic time derivative $\left[\frac{d}{dt}\log\|\omega\|_\infty\right]^{-1}$ and its line fitting $\hat{\gamma}_1^{-1}(\hat{t}_s - t)$, computed on the 2048×2048 mesh.

Applying the Ideas: Computing the Line Fitting

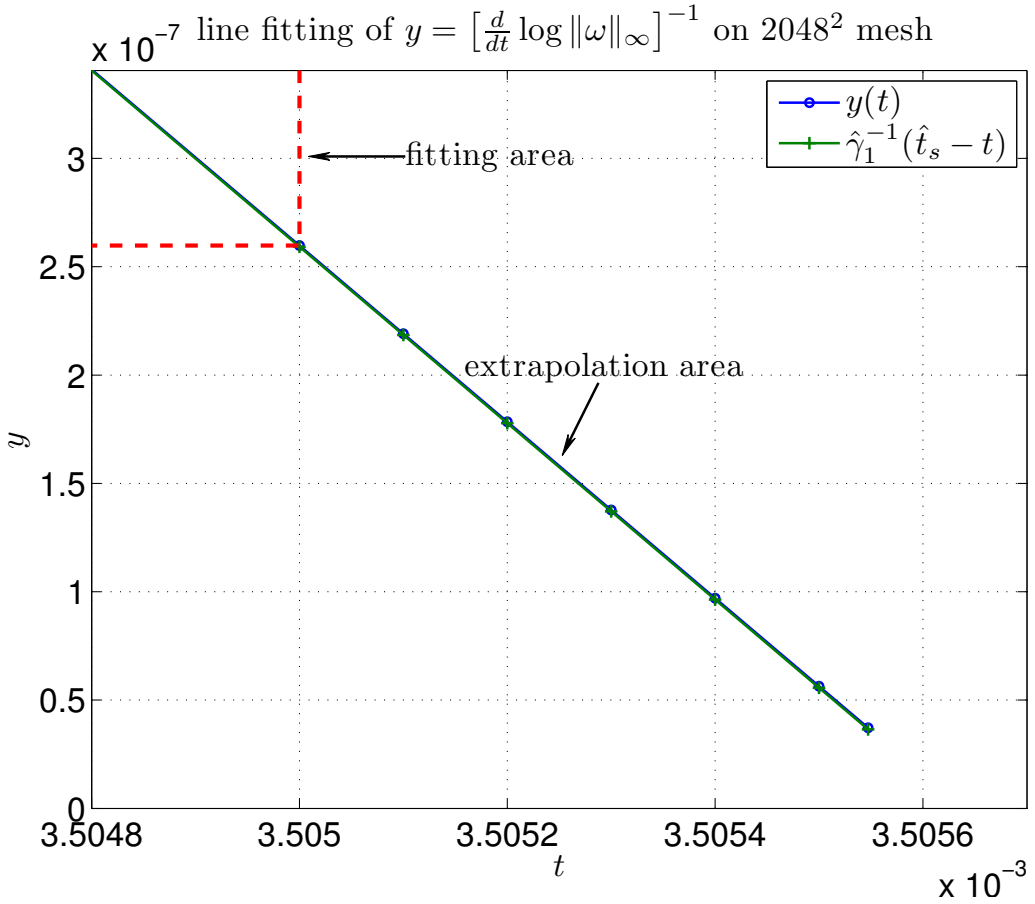

Figure : A zoom-in view of the line fitting $\hat{\gamma}_1^{-1}(\hat{t}_s - t)$.

Applying the Ideas: Computing the Line Fitting

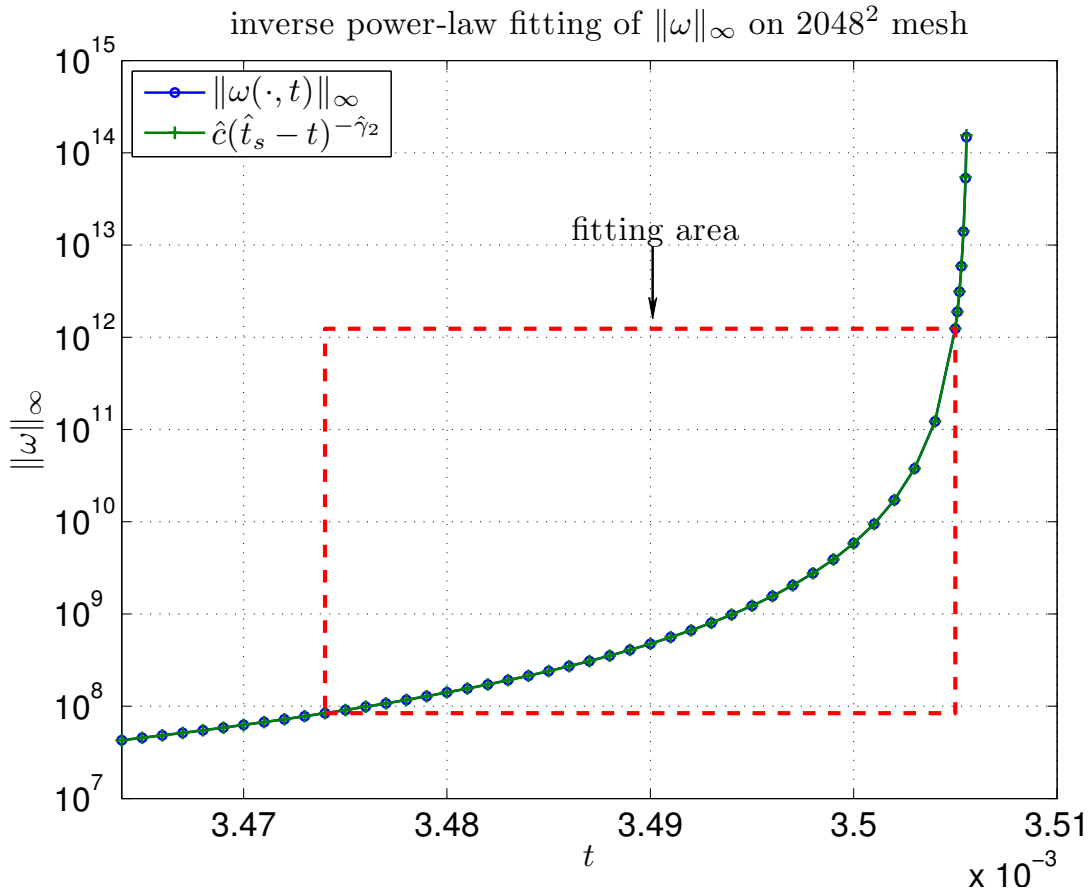

Figure : Maximum vorticity $\|\omega\|_\infty$ and its inverse power-law fitting $\hat{c}(\hat{t}_s - t)^{-\hat{\gamma}_2}$, computed on the 2048×2048 mesh.

Applying the Ideas: the "Best" Fitting Interval

Table : The "best" fitting interval $[\tau_1, \tau_2]$ and the estimated singularity time $\hat{t}_s$.

Mesh size	τ_1	τ_2	$\hat{t}_s$
1024×1024	0.003306	0.003410	0.0035070
1280×1280	0.003407	0.003453	0.0035063
1536×1536	0.003486	0.003505	0.0035056
1792×1792	0.003479	0.003505	0.0035056
2048×2048	0.003474	0.003505	0.0035056

Applying the Ideas: Results of the Line Fitting

Table : The best line fittings for $\|\omega\|_\infty$ computed on $[\tau_1, \tau_2]$.

Mesh size	$\hat{\gamma}_1^\dagger$	$\hat{\gamma}_2^\ddagger$	$\hat{c}$
1024×1024	2.5041	2.5062	4.8293×10^{-4}
1280×1280	2.4866	2.4894	5.5362×10^{-4}
1536×1536	2.4544	2.4559	7.4912×10^{-4}
1792×1792	2.4557	2.4566	7.4333×10^{-4}
2048×2048	2.4568	2.4579	7.3273×10^{-4}

$\dagger$: $\hat{\gamma}_1$ is computed from $\left[\frac{d}{dt}\log\|\omega\|_\infty\right]^{-1} \sim \gamma^{-1}(t_s - t)$.

$\ddagger$: $\hat{\gamma}_2$ is computed from $\log\|\omega\|_\infty \sim -\gamma \log(\hat{t}_s - t) + \log c$.

Conclusion: the maximum vorticity develops a singularity $\|\omega\|_\infty \sim c(t_s - t)^{-\gamma}$ at $t_s \approx 0.0035056$ (recall $t_e \approx 0.00350555$)

Comparison with Other Numerical Studies

Table : Comparison of our results with other numerical studies. K: Kerr (1993); BP: Boratav and Pelz (1994); GMG: Grauer et al. (1998); OC: Orlandi and Carnevale (2007); τ_2: the last time at which the solution is deemed "well resolved".

Studies	τ_2	t_s	Effec. res.	Vort. amp.
K	17	18.7	$\leq 512^3$	23
BP	$1.6^\dagger$	2.06	1024^3	180
GMG	1.32	1.355	2048^3	21
OC	2.72	2.75	1024^3	55
Ours	0.003505	0.0035056	$(3 \times 10^{12})^2$	3×10^8

†: According to Hou and Li (2008).

Nonlinear alignment of vortex stretching

- The vorticity direction $\xi = \omega/|\omega|$ could also play a role!
- Recall the vorticity equation

$$|\omega|_t + u \cdot \nabla |\omega| = \alpha |\omega|,$$

where $\alpha = \xi \cdot \nabla u \cdot \xi$ is the vorticity amplification factor

$$\alpha = \xi \cdot \nabla u \cdot \xi = \xi \cdot S\xi, \qquad S = \frac{1}{2}(\nabla u + \nabla u^T),$$

thus the growth of α depends on the eigenstructure of S

Spectral Dynamics

- Due to symmetry, S has
  - 3 real eigenvalues $\{\lambda_i\}_{i=1}^3$ (assuming $\lambda_1 \geq \lambda_2 \geq \lambda_3$), and
  - a complete set of orthogonal eigenvectors $\{w_i\}_{i=1}^3$
- We discover, at the location of the maximum vorticity, that:
  - the vorticity direction ξ is perfectly aligned with w_2, i.e.

$$\lambda_2 = \alpha = \frac{d}{dt} \log \|\omega\|_\infty \sim c_2 (t_s - t)^{-1}$$

  - the largest positive/negative eigenvalues satisfy

$$\lambda_{1,3} \sim \pm \frac{1}{2} \|\omega\|_\infty \sim \pm c (t_s - t)^{-2.457}$$

The DHY Non-blowup Criterion

- Essential ideas of DHY: no blowup if, among other things,
  - the divergence of ξ, $\nabla \cdot \xi$, and
  - the curvature $\kappa = |\xi \cdot \nabla \xi|$,

  along a vortex line do not grow "too fast" compared with the "diminishing rate" of the length of the vortex line
- Similar in spirit to CFM but more localized

Checking Against the DHY Criterion

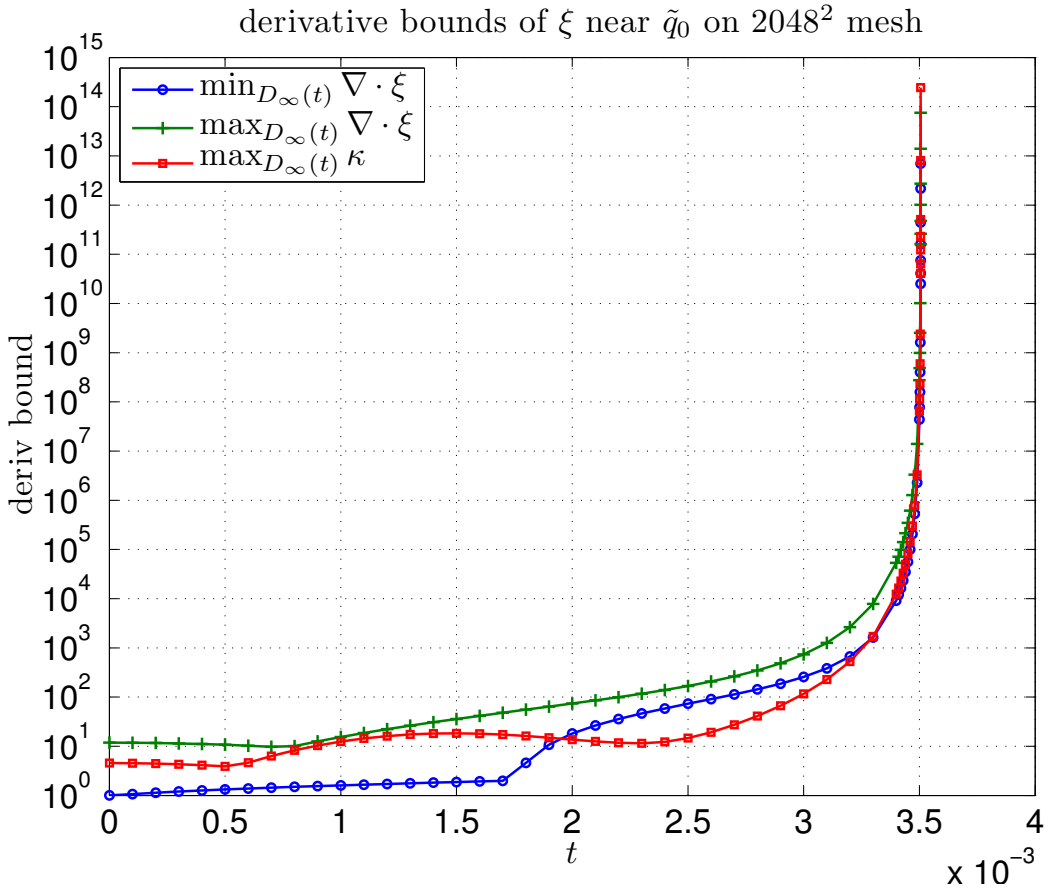

Figure : The maximum/minimum of $\nabla \cdot \xi$ and κ in a local neighborhood $D_\infty(t)$ of the maximum vorticity.

Geometry of the Vorticity Direction (Cont'd)

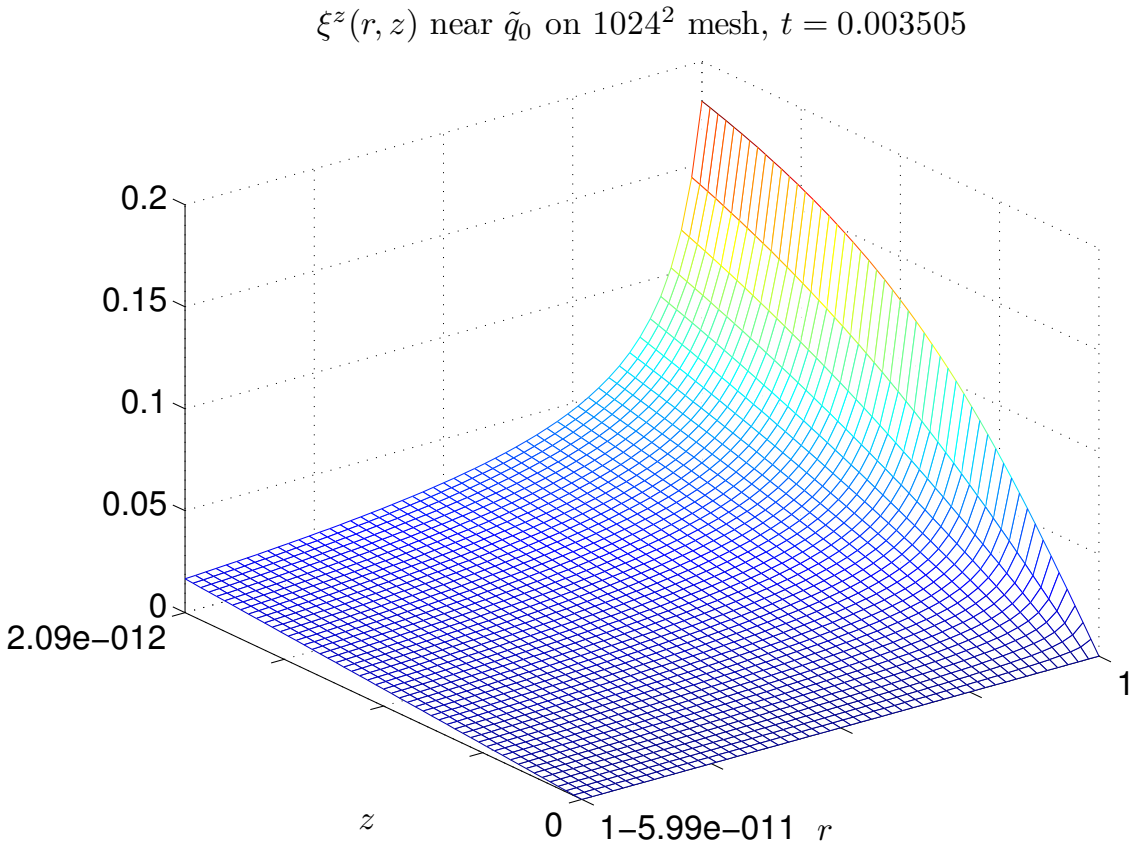

Figure : The z-component ξ^z of the vorticity direction ξ near the maximum vorticity. Note the rapid variation of ξ^z in z.

Outline

Locally Self-Similar Solutions

- Solutions of the 3D Euler equations in $\mathbb{R}^3$ have special scaling properties:

$$u(x,t) \longrightarrow \lambda^{\alpha} u(\lambda x, \lambda^{\alpha+1} t), \qquad \lambda > 0,\ \alpha \in \mathbb{R}$$

- Can this give rise to a (locally) self-similar blowup?

$$\nabla u(x,t) \sim \frac{1}{t_s - t} \nabla U\left(\frac{x - x_0}{[t_s - t]^{\beta}}\right), \qquad x \in \mathbb{R}^3$$

- Recent results by D. Chae (2007,2010,2011) seem to give a negative answer under some strong (exponential) decay assumption on the self-similar profile ∇U.

Self-Similar Solutions with Axis-Symmetry

- In axisymmetric flows, self-similar solutions naturally take the form

$$u_1(\tilde{x},t) \sim (t_s - t)^{\gamma_u} U\left(\frac{\tilde{x} - \tilde{x}_0}{\ell(t)}\right),$$
$$\omega_1(\tilde{x},t) \sim (t_s - t)^{\gamma_\omega} \Omega\left(\frac{\tilde{x} - \tilde{x}_0}{\ell(t)}\right),$$
$$\psi_1(\tilde{x},t) \sim (t_s - t)^{\gamma_\psi} \Psi\left(\frac{\tilde{x} - \tilde{x}_0}{\ell(t)}\right), \qquad \tilde{x} \to \tilde{x}_0,\ t \to t_s^-,$$

where $\tilde{x} = (r,z)^T$ and $\ell(t) \sim [\delta^{-1}(t_s - t)]^{\gamma_\ell}$ is a length scale, and the exponents satisfy

$$\gamma_\omega = -1, \qquad \gamma_\psi = -1 + 2\gamma_\ell, \qquad \gamma_u = -1 + \frac{1}{2}\gamma_\ell.$$

This would give rise to $\|\nabla u(\cdot,t)\|_\infty \sim c(t_s - t)^{\gamma_u - \gamma_\ell}$.

Identifying a Self-Similar Solution

- We remark that the recent result of Chae-Tsai on non-existence of self-similar solutions of 3D axisymmetric Euler does not apply to our solution since they assume $|U(\xi)| \to 0$ as $|\xi| \to \infty$.
- In our case, we found that $U(0) = \Psi(0) = \Omega(0) = 0$, and $|U(\xi)| \approx c_0|\xi|^\beta$ for some $0 < \beta < 1$ as $|\xi| \to \infty$, where β satisfies $\gamma_u = \gamma_\ell \beta$ with $\gamma_u > 0$ and $\gamma_\ell > 0$. This gives $u(1, z, t_s) \approx c_0 z^\beta$ at the singularity time.
- To identify a "self-similar neighborhood", consider

$$C_\infty(t) = \left\{ (r, z) \in D \colon |\omega(r, z, t)| = \tfrac{1}{2}\|\omega(\cdot, t)\|_\infty \right\}$$

Existence of Self-Similar Neighborhood

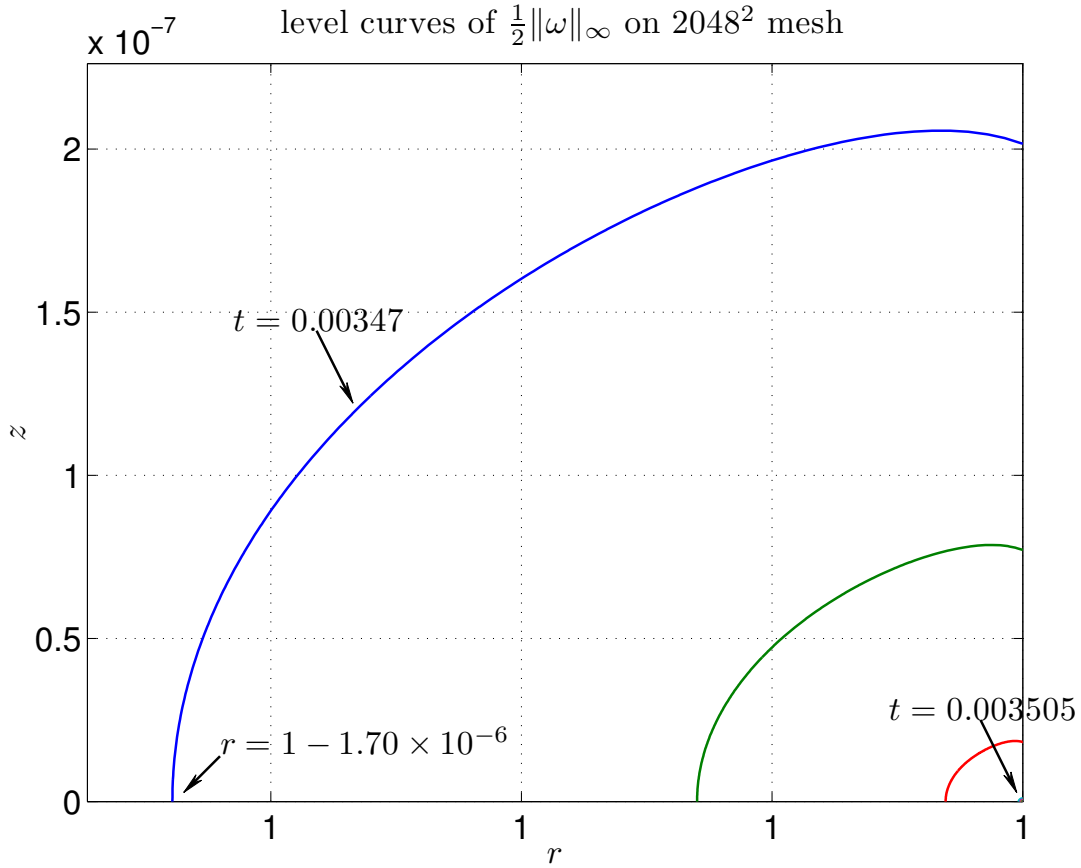

Figure : The level curves of $\frac{1}{2}\|\omega\|_\infty$ in linear-linear scale at various time instants.

Existence of Self-Similar Neighborhood (Cont'd)

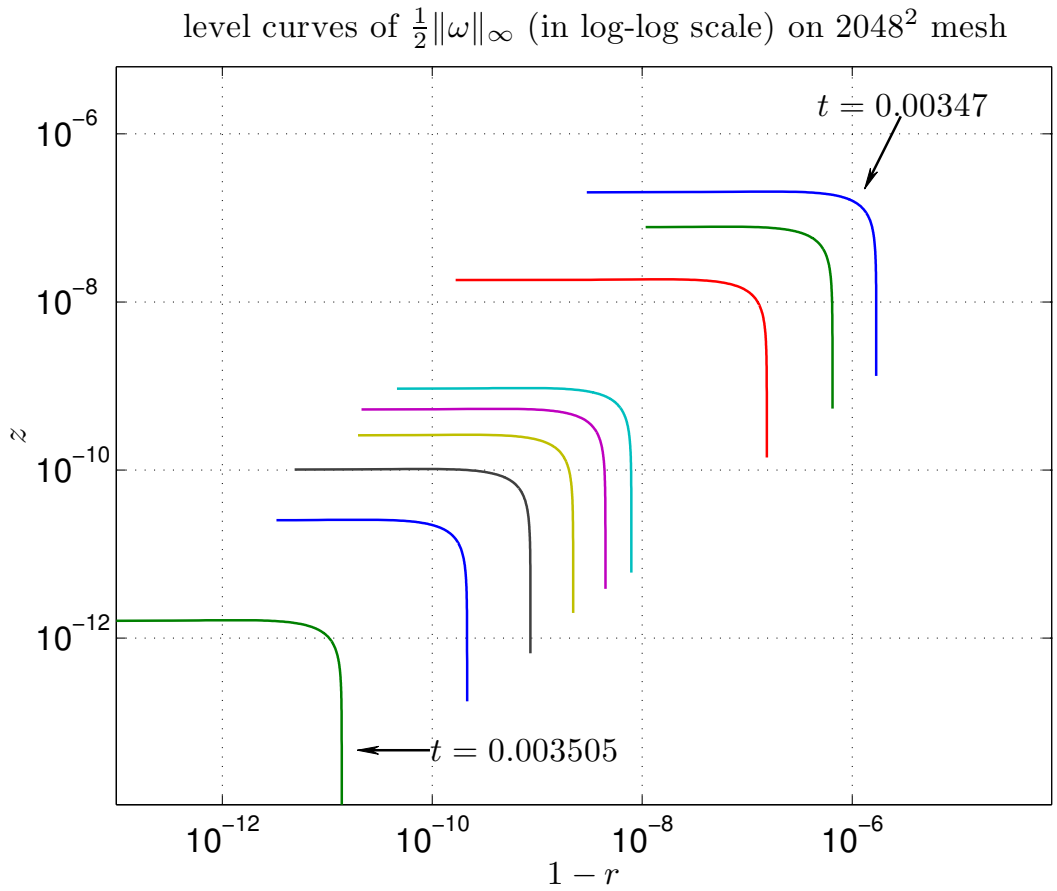

Figure : The level curves of $\frac{1}{2}\|\omega\|_\infty$ in log-log scale (against the variables $1 - r$ and z) at various time instants. Note the similar shapes of all curves.

Existence of Self-Similar Neighborhood (Cont'd)

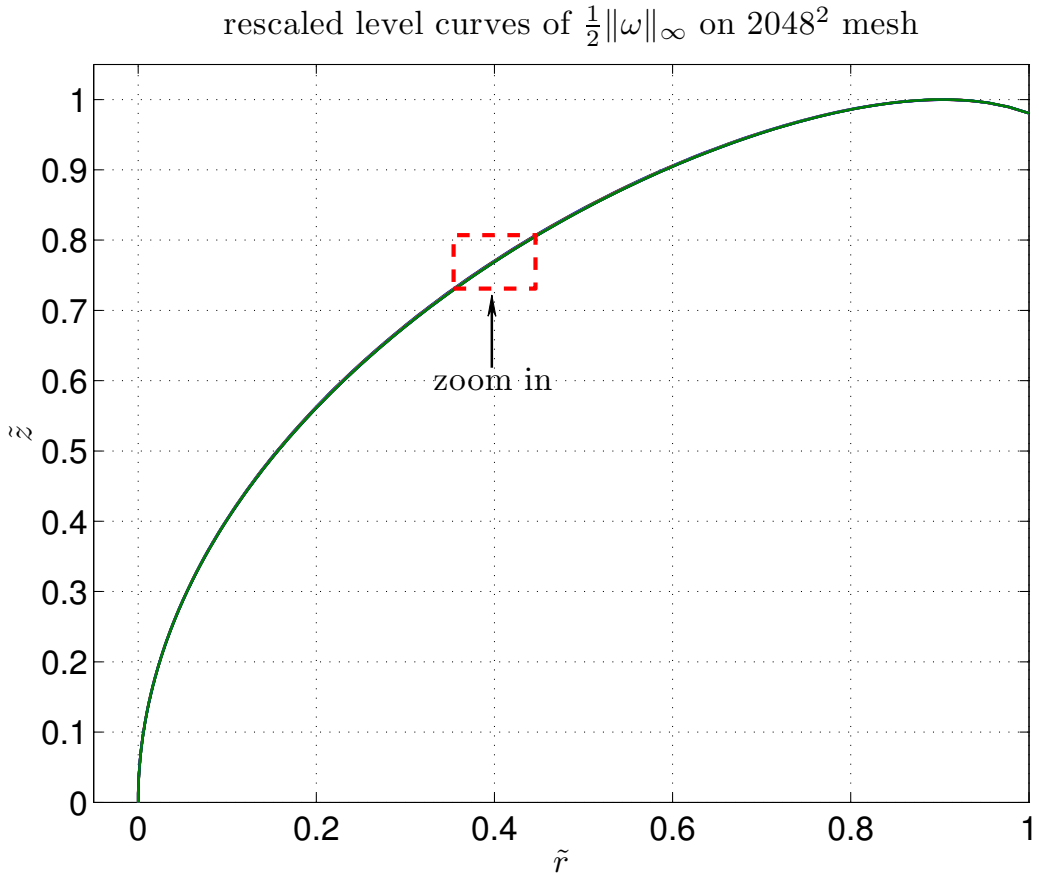

Figure : The rescaled level curves of $\frac{1}{2}\|\omega\|_\infty$.

The Scaling Exponents

Table : Scaling exponents of ℓ, u_1, ω_1, and ψ_1.

Mesh size	$\hat{\gamma}_\ell$	$\hat{\gamma}_u$	$\hat{\gamma}_\omega$	$\hat{\gamma}_\psi$
1024×1024	2.7359	0.4614	-0.9478	4.7399
1280×1280	2.9059	0.4629	-0.9952	4.8683
1536×1536	2.9108	0.4600	-0.9964	4.8280
1792×1792	2.9116	0.4602	-0.9966	4.8294
2048×2048	2.9133	0.4604	-0.9972	4.8322

$\gamma_\ell \geq 1$: consistent with the *a posteriori* bound $\|u\|_\infty \leq C$

Consistency Check

Table : Consistency check for the scaling exponents.

Mesh size	$-1+\frac{1}{2}\hat{\gamma}_\ell$	$-1+2\hat{\gamma}_\ell$	$\hat{\gamma}_u-\hat{\gamma}_\ell$
1024×1024	0.3679	4.4717	-2.2745
1280×1280	0.4530	4.8118	-2.4430
1536×1536	0.4554	4.8215	-2.4508
1792×1792	0.4558	4.8232	-2.4514
2048×2048	0.4567	4.8266	-2.4529
Ref. value	$\hat{\gamma}_u$: 0.4604	$\hat{\gamma}_\psi$: 4.8322	$\hat{\gamma}_1$: 2.4568

$\|\omega\|_\infty \sim c(t_s-t)^{-2.45}$: consistent with Chae's nonexistence results

1D Models

One can rewrite the Euler equations as follows:

$$(r^2 u_1)_t + u^r (r^2 u_1)_r + u^z (r^2 u_1)_z = 0,$$
$$\omega_{1,t} + u^r \omega_{1,r} + u^z \omega_{1,z} = (u_1^2)_z,$$
$$-[\partial_r^2 + (3/r)\partial_r + \partial_z^2]\psi_1 = \omega_1.$$

The 1D models based on this new singularity formation scenario are proposed and investigated by restricting the 3D Euler equations on $r = 1$:

$$w_t(z,t) + u(z,t) w_z(z,t) = \theta_z(z,t),$$
$$\theta_t(z,t) + u(z,t)\theta_z(z,t) = 0,$$

where $w = \omega_1$, $u = u^z$ and $\theta = u_1^2$. The above equations are exact and can also be viewed as restriction of the Boussinesq equations on $r = 1$:

$$w_t + \mathbf{u} \cdot \nabla w = \theta_z,$$
$$\theta_t + \mathbf{u} \cdot \nabla \theta = 0,$$
$$\mathbf{u} = \nabla^T \phi, \quad -\Delta \phi = w.$$

The Biot-Savart Laws

To close the 1D system, one needs appropriate Biot-Savart law that connects the velocity $u(z)$ to the vorticity $w(z)$:

- The Hou-Luo model [T.Y. Hou, G. Luo, 2013] preserves the symmetry of the Euler equations:

$$u_z(z) = \mathcal{H}w = \mathrm{P.V.}\frac{1}{2}\int_{-1}^{1} w(y)\cot[\frac{\pi}{2}(z-y)]\mathrm{d}y.$$

- The Choi-Kiselev-Yao model [K.Choi, A. Kiselev, Y. Yao, 2014] further simplifies the HL model:

$$u(z) = -z\int_{z}^{1} w(y)/y\mathrm{d}y.$$

- One can verify that the CKY model is indeed a leading order approximation to the HL model near the origin

$$u_{HL}(z) - u_{CKY}(z) = O(z^2).$$

Comparison between the 1D model and the 3D Euler

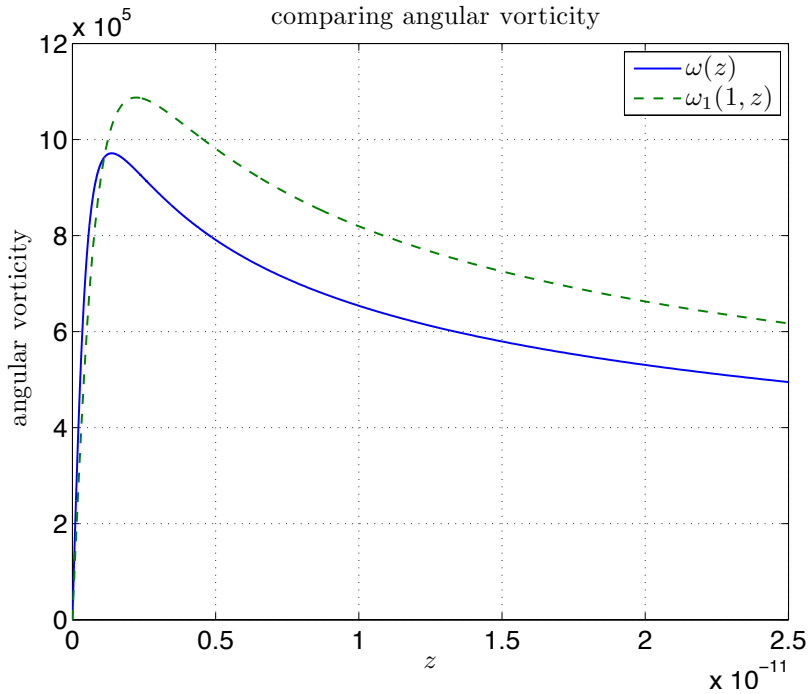

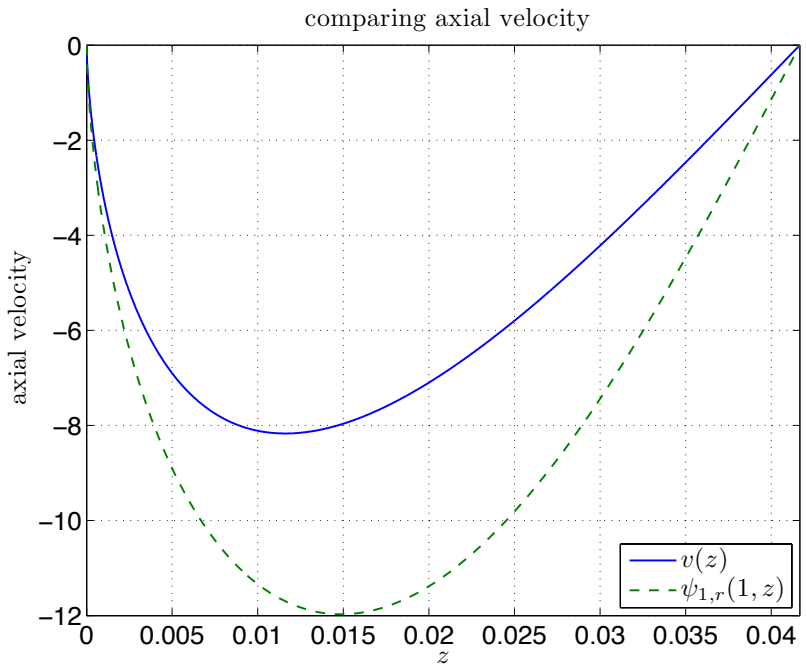

Comparison of numerical solutions of the 1D model with 3D Euler. (a) angular vorticity, and (b) axial velocity.

1D Models-continued

The finite-time singularity of the CKY model is proved by Choi, Kiselev and Yao [2014]. And the singularity of the HL model is proved very recently by Choi, Hou, Luo, Sverak, Kiselev and Yao[2014].

Lemma 1 Let $\omega \in H^1$ be odd at $z = 0$ and let $u_z = H(\omega)$ the velocity field. Then for any $z \in [0, L/2]$,

$$u(z)\cot(\mu z) = -\frac{1}{\pi}\int_0^{L/2} K(z,z')\omega(z')\cot(\mu z')\,dz', \tag{1}$$

where $\mu = \pi/L$ and

$$K(x,y) = s\log\left|\frac{s+1}{s-1}\right| \qquad \text{with} \qquad s = s(x,y) = \frac{\tan(\mu y)}{\tan(\mu x)}. \tag{2}$$

Furthermore, the kernel $K(x,y)$ has the following properties:

1. $K(x,y) \geq 0$ for all $x,\ y \in (0, \frac{1}{2}L)$ with $x \neq y$;
2. $K(x,y) \geq 2$ and $K_x(x,y) \geq 0$ for all $0 < x < y < \frac{1}{2}L$;
3. $K(x,y) \geq 2s^2$ and $K_x(x,y) \leq 0$ for all $0 < y < x < \frac{1}{2}L$.

Blow-up of the 1D model

The main blow-up result is stated in the following theorem:

Theorem 1 (Choi, Hou, Kiselev, Luo, Sverak and Yao) For any initial data $\rho_0 \in H^2,\ \omega_0 \in H^1$ such that

(i) ρ_0 is even and ω_0 is odd at $z = 0,\ \frac{1}{2}L$,

(ii) $\rho_{0z},\ \omega_0 \geq 0$ on $[0, \frac{1}{2}L]$, and

(iii) $\int_0^{L/2} \left[\rho_0(z) - \rho_0(0)\right]^2 dz > 0$, then the solution of the 1D model develops a singularity in finite time.

One can show that the solution of the 1D model satisfies:

1. ρ is even and $\omega,\ u$ are odd at $z = 0,\ \frac{1}{2}L$ for all $t \geq 0$;
2. $\rho_z,\ \omega \geq 0$ and $u \leq 0$ on $[0, \frac{1}{2}L]$ for all $t \geq 0$.

Sketch of the proof – continued

To prove the finite-time blowup, we define

$$I(t) := \int_0^{L/2} \rho(z,t)\cot(\mu z)\,dz. \tag{3}$$

and obtain

$$\begin{aligned}\frac{d}{dt}I(t) &= -\int_0^{L/2} u(x)\rho_x(x)\cot(\mu x)\,dx \\ &= \frac{1}{\pi}\int_0^{L/2}\rho_x(x)\int_0^{L/2}\omega(y)\cot(\mu y)K(x,y)\,dy\,dx,\end{aligned}$$

where we have used the representation formula (1) from Lemma 1.

By the assumption on the initial data, we have $\rho_x,\ \omega \geq 0$ on $[0, \frac{1}{2}L]$. Moreover, from Lemma 1, we have $K \geq 0$ for $y < x$, and $K \geq 2$ for $y > x$. Thus, we get

$$\frac{d}{dt}I(t) \geq \frac{2}{\pi}\int_0^{L/2}\rho_x(x)\int_x^{L/2}\omega(y)\cot(\mu y)\,dy\,dx.$$

Sketch of the proof – continued

It remains to find a lower bound for the right hand side, which involves some delicate dynamic estimates using the w-eqn. We can show that

$$\begin{aligned}
\frac{d}{dt} I(t) &\geq \frac{2}{\pi} \int_0^t \int_0^{L/2} \rho_y(y,s) \cot(\mu y) \int_0^{\tilde{\zeta}(t)} \rho_x(x,t)\, dx\, dy\, ds \\
&= \frac{2}{\pi} \int_0^t \int_0^{L/2} (\rho\rho_y)(y,s) \cot(\mu y)\, dy\, ds \\
&= \frac{\mu}{\pi} \int_0^t \int_0^{L/2} \rho^2(y,s) \csc^2(\mu y)\, dy\, ds \\
&\geq \frac{\mu}{\pi} \int_0^t \int_0^{L/2} \rho^2(y,s) \cot^2(\mu y)\, dy\, ds \\
&\geq \frac{2\mu}{\pi L} \int_0^t \left(\int_0^{L/2} \rho(y,s) \cot(\mu y)\, dy \right)^2 ds = \frac{2}{L^2} \int_0^t I^2 ds.
\end{aligned}$$

Self-similar Singularity

The two models enjoy the following scaling-invariant property, which is the same as the Euler equations

$$w(x,t) \to \frac{1}{\mu} w(\frac{x}{\lambda}, \frac{t}{\mu}), \quad u(x,t) \to \frac{\lambda}{\mu} u(\frac{x}{\lambda}, \frac{t}{\mu}), \quad \theta(x,t) \to \frac{\lambda}{\mu^2} \theta(\frac{x}{\lambda}, \frac{t}{\mu}).$$

And their singular solutions both develop self-similar structure around their singularity points. We make the following self-similar ansatz:

$$w(z,t) \approx (T-t)^{c_w} W(\frac{z}{(T-t)^{c_l}}),$$

$$\theta(z,t) \approx (T-t)^{c_\theta} \Theta(\frac{z}{(T-t)^{c_l}}),$$

$$u(z,t) \approx (T-t)^{c_u} U(\frac{z}{(T-t)^{c_l}}).$$

Self-similar Equations

Plugging the ansatz of the solutions into the equations and matching the exponents of the $(T-t)$, we get

$$c_w = -1, \quad c_u = c_l - 1, \quad c_\theta = c_l - 2,$$

and the following self-similar equations that govern the profiles $W(\xi)$, $U(\xi)$ and $\Theta(\xi)$ in the singular solutions,

$$W(\xi) + c_l \xi W_\xi(\xi) + U(\xi) W_\xi(\xi) = \Theta_\xi(\xi),$$
$$(2 - c_l)\Theta(\xi) + c_l \xi \Theta_\xi(\xi) + U(\xi)\Theta_\xi(\xi) = 0.$$

The Biot-Savart laws become

$$U_{HL}(\xi) = \frac{1}{\pi} \int_0^\infty \ln \left| \frac{\xi - \eta}{\xi + \eta} \right| W(\eta) \mathrm{d}\eta, \quad U_{CKY}(\xi) = -\xi \int_\xi^\infty \frac{W(\eta)}{\eta} \mathrm{d}\eta.$$

Self-similar Equations-continued

- The self-similar singularity of the two 1D models are of the **second kind**, since the scaling exponent c_l cannot be simply determined by symmetry or the conservation of energy.
- Solving the self-similar equations is essentially **a nonlinear eigenvalue problem**. Namely, one needs to find the scaling exponent c_l such that the equations have non-trivial solutions.
- The self-similar equations have non-linear and non-local features, which make the problem difficult to solve.

Outline

Self-similar Equations for the CKY Model

The Biot-Savart law in the CKY model

$$U_{CKY}(\xi) = -\xi \int_{\xi}^{\infty} \frac{W(\eta)}{\eta} \mathrm{d}\eta$$

can be decomposed as a local relation with a global constraint

$$\left(\frac{U(\xi)}{\xi}\right)' = \frac{W(\xi)}{\xi}$$
$$\lim_{\xi \to \infty} \frac{U(\xi)}{\xi} = 0.$$

This decomposition allows us to construct the profiles using the local relation, and then determine c_l using the global constraint.

Construct Near-field Solution

Neglecting the global constraint in the Biot-Savart law, the self-similar equations become an ODE system

$$\Theta'(\xi) = \frac{(c_l - 2)\Theta(\xi)}{U(\xi) + c_l\xi},$$
$$W'(\xi) = \frac{(c_l - 2)\Theta(\xi)}{(c_l\xi + U(\xi))^2} - \frac{W(\xi)}{c_l\xi + U(\xi)},$$
$$\left(\frac{U(\xi)}{\xi}\right)' = \frac{W(\xi)}{\xi}.$$

The RHS of the above ODE system has a formal singularity at $\xi = 0$, so the classical existence and uniqueness result does not apply.

Construct Near-field Solution-continued

We use the power series method to construct local self-similar profiles

$$W(\xi)=\sum_{i=1}^{\infty} W_i\xi^i,\ U(\xi)=\sum_{i=1}^{\infty} U_i\xi^i,\ \Theta(\xi)=\sum_{i=s}^{\infty}\Theta_i\xi^i,$$

where s is the leading order of $\Theta(\xi)$ at the origin. Plugging the power series into the self-similar equations, we get the following:

$$(2-c_l+sc_l+sU_1)\Theta_s=0 \quad \longrightarrow \quad U_1=\frac{(1-s)c_l-2}{2}.$$

For $k>s$, $c_l>2$

$$\Theta_k=\frac{-\sum_{m=s}^{k-1}U_m(k-m+1)\Theta_{k-m+1}}{(k/s-1)(c_l-2)},$$

$$U_k=\frac{k\Theta_k-\sum_{m=s}^{k-1}U_m(k-m)^2U_{k-m+1}}{(k-1)+(c_l/s-2/s)(k-1)^2}.$$

Note that the denominators are positive, which we will come back to later.

Near-field Solutions

We get the following conclusion for the near-field power series solutions:

- For fixed $c_I > 2$ and the leading order $s \geq 2$, the power series can actually be uniquely (up to re-scaling) determined.
- Using a majorization argument, we get a quantitative estimates of the coefficients and show that the power series converge on $(0, \epsilon)$. We have $W(\xi) > 0$, $U(\xi) < 0$, $\Theta(\xi) > 0$.

Remark 1 $c_\theta = c_I - 2$, and θ is convected by the velocity thus cannot blowup, so we require that $c_I > 2$.

Remark 2 Since $\theta(z, t)$ is advected by the velocity field, the leading order of $\theta(z, t)$ at $z = 0$, s, is preserved. We will see later in our numerical results that s actually determines the profiles of the singular solutions.

Extending the Local Self-similar Profiles

We consider extending the self-similar profiles by solving the nonlinear ODE system. We get the following results.

- The profile $\Theta(\xi)$ remain positive, according to

$$\Theta'(\xi) = \frac{(c_l - 2)\Theta(\xi)}{U(\xi) + c_l\xi},$$

- The profile $W(\xi)$ remains positive, according to

$$W'(\xi) = \frac{(c_l - 2)\Theta(\xi)}{(c_l\xi + U(\xi))^2} - \frac{W(\xi)}{c_l\xi + U(\xi)},$$

- $U(\xi)/\xi + c_l$ is increasing and positive, according to

$$\left(\frac{U(\xi)}{\xi}\right)' = \frac{W(\xi)}{\xi}.$$

- Using the above *a priori* estimates, we can show that the local self-similar profiles can be extended to the whole R^+.

The Global Constraint in the Biot-Savart Law

Recall that in our construction of the self-similar profiles, we have neglected the global constraint in the Biot-Savart law,

$$G(c_l) \equiv \lim_{\xi \to \infty} U(\xi)/\xi = 0.$$

For fixed leading order of $\Theta(\xi)$, s, our constructed self-similar profiles only depend on c_l. We define function $G(c_l)$ as the limit of the self-similar profile $U(\xi)/\xi$ for scaling exponent c_l. We have the following results.

- Using an iterative argument, we can get sharper and shaper estimates of the profiles, and finally get that $U(\xi)/\xi$ converge to $G(c_l) < +\infty$ uniformly for $c_l > 2$ in a closed interval. (see the next slide)
- Using the above uniform convergence and the continuous dependence of ODE solutions on parameters, we get that $G(c_l) \in C((2, +\infty))$.

Continuity of $G(c_l)$

- **Lemma** $G(c_l) = \lim_{\xi\to\infty} U(\xi)\xi^{-1} > -2$.
  Otherwise $\Theta(\xi) > C\xi \ \to \ W(\xi) > C \to \lim_{\xi\to+\infty} U(\xi)/\xi = +\infty$.
- $U(\xi_0) > (-2+\epsilon)\xi_0 \ \to \ \Theta(\xi) > C\xi^{1-\epsilon/c_l} \ \to W(\xi) < C$.
- $W(\xi) < C \ \to U(\xi) < C\xi \ln \xi \ \to \ W(\xi) < C(\ln \xi)^{-1}$.
- $W(\xi) < C(\ln \xi)^{-1} \ \to \ U(\xi) < C\xi \ln\ln \xi$.
  $U(\xi) < C\xi \ln\ln \xi \to W(\xi) < C\exp(-C(\ln \xi)^{\alpha})$.

We get shaper and shaper estimates of $W(\xi)$ by analyzing the nonlinear interaction in the self-similar equations. With $W(\xi) < C\exp(-C(\ln \xi)^{\alpha})$ we can get that $U(\xi)\xi^{-1}$ converge uniformly for c_l in local closed interval.

Determine the scaling exponent c_l

With our previous construction, to prove the existence of solutions to the self-similar equations, we need to show that there exist a solution to

$$G(c_l) = 0.$$

Using the continuity of $G(c_l)$ and the intermediate value theorem, we only need to show that there exist $c_l^l, c_l^r > 2$, such that

$$G(c_l^l) < 0, \quad G(c_l^r) > 0.$$

Due to the nonlinearity of the self-similar equations, it is not easy to verify the above condition directly. And we achieve this with the assistance of numerical computation, namely, we use computer-assisted proof.

A Computer-verifiable Condition

$G(c_l)$ is defined as the limit $\lim_{\xi\to\infty} \frac{U(\xi)}{\xi}$, and we cannot solve the ODE system up to $+\infty$ to estimate $G(c_l)$. We use the following Lemma.

Lemma: *At* $\xi_0 > 0$, *if*

$$U(\xi_0) > 0,$$

then $G(c_l) > 0$;
if

$$\frac{U(\xi_0)}{\xi_0} > -2,\ U(\xi_0)/\xi_0 + c_l W(\xi_0) + \frac{c_l(c_l-2)\xi_0\Theta(\xi_0)}{(U(\xi_0)+2\xi_0)(c_l\xi_0+U(\xi_0))} < 0,$$

then $G(c_l) < 0$.

Our strategy is the following: We first numerically construct the near-field self-similar profiles using the truncated power series solutions, and then extend the local profiles to some ξ_0 by solving the nonlinear ODE system. Finally we employ the above Lemma to verify the sign of $G(c_l)$.

Far-field Property of the Self-similar Profiles

Using the above strategy, we can verify the existence of solution to $G(c_l)$ and prove the existence of solutions to the self-similar equations. After we get the solutions, we further analyze their properties at $+\infty$.

- By introducing a new variable $\zeta = \xi^{-1/c_l}$ and considering the ODE system under the variable ζ, we can show that $U(\xi)/\xi$, $W(\xi)$ and $\Theta(\xi)/\xi$ are smooth functions of ζ using a bootstrap argument.
- Then using an uniqueness argument, one can actually show that $U(\xi)/\xi$, $W(\xi)$, $\Theta(\xi)$ are analytic functions of ζ.

Specifically, we have

$$W(\xi) = O(\xi^{-1/c_l}), \quad U(\xi) = O(\xi^{1-1/c_l}), \quad \Theta(\xi) = O(\xi^{1-\frac{2}{c_l}}), \quad \xi \to +\infty.$$

Comments on the Far-field Property of the Profiles

Remark 1 The above results imply that $U(\xi) = O(\xi^{1-1/c_l})$, thus

$$u(x, T^-) \approx (T-t)^{c_l-1} U(\frac{x}{(T-t)^{c_l}}) \approx C x^{1-1/c_l}.$$

Namely the velocity field is Hölder continuous at the singularity time, which agrees with our numerical simulation. Such behavior is also observed in the simulation of Luo and Hou for the 3D Euler equations. vskip 0.3cm It should be no surprise that we get $U(\xi) = O(\xi^{1-1/c_l})$. Actually, based on the above self-similar ansatz, this is the only possible growth rate such that $u(x, T^{-1})$ remains bounded away from the singularity point.

Existence of Self-similar Profiles

We verify the existence of root to $G(c_l) = 0$ for $s = 2, 3, 4, 5$, and thus complete the following Theorem:

Theorem *There exist a discrete family of self-similar profiles for the CKY model, which correspond to different leading orders of the profile* $\Theta(\xi)$ *at the origin,* $s = 2, 3, 4, 5$. *The self-similar profiles are analytic with respect to* ξ *at the origin* $\xi = 0$. *Moreover* $U(\xi)/\xi$, $W(\xi)$ *and* $\Theta(\xi)/\xi$ *are analytic with respect to* $\zeta = \xi^{-1/c_l}$ *at* $\zeta = 0$.

Remark Our proof relies on the local nature of the Biot-Savart law, thus cannot be generated to the HL model or the 3D Euler equations.

Comparison with Direct Numerical Simulation

We compare the scaling exponents obtained from direct numerical simulation of the CKY model and the solving the self-similar equations.

	$s=2$	$s=3$	$s=4$	$s=5$
Direct Simulation	3.7942	3.3143	3.1718	3.0773
Self-similar Equations	3.7967	3.3157	3.1597	3.0841

Table : c_l Table.

	$s=2$	$s=3$	$s=4$	$s=5$
Direct Simulation	-0.9747	-1.0001	-1.0006	-1.0007
Self-similar Equations	-1	-1	-1	-1

Table : c_w Table.

Comparison of the Self-similar Profiles

We compare the self-similar profiles obtained from rescaling the singular numerical solutions and from the self-similar equations.

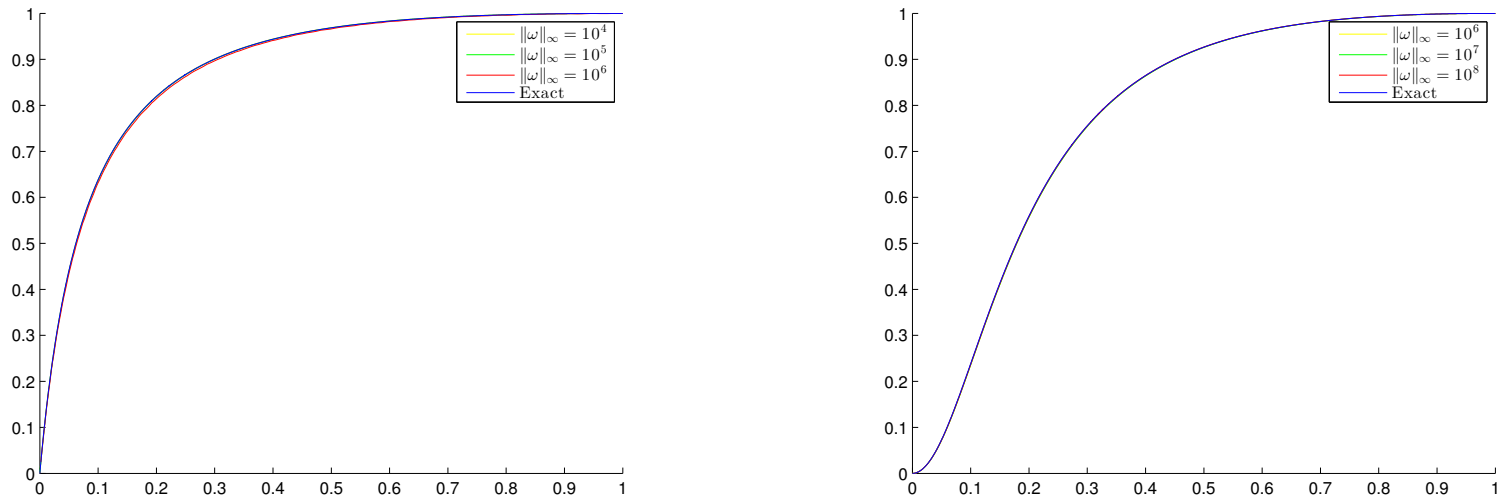

Figure : Self-similar profiles for $s = 2$ and $s = 3$ respectively.

We can see that the self-similar profiles we find are consistent with those obtained from direct numerical simulation.

Summary

- Main contributions of our study: discovery of potentially singular solutions of the 3D Euler equations
- Similar singularity formation also observed in 2D Boussinesq equations for stratified flows
- The singularity occurs at a stagnation point where the effect of convection is minimized.
- Strong symmetry of the solution plus the presence of the physical boundary seem to play a crucial in generating a stable and substainable locally self-similar blowup.
- Analysis of the corresponding 1D model sheds new light to the blowup mechanism.
- Analysis of the 2D Boussinesq and 3D Euler is more challenging and is under investigation.

References

- G. Luo and T. Y. Hou, *Potentially Singular Solutions of the 3D Axisymmetric Euler Equations,*, PNAS, Vol. 111, no. 36, pp. 12968-12973, 2014. Doi: 10.1073/pnas.1405238111
- G. Luo and T. Y. Hou, *Toward the Finite-Time Blowup of the 3D Incompressible Euler Equations: a Numerical Investigation*. MMS, Vol. 12 (4), pp. 1722-1776, 2014. DOI. 10.1137/140966411.
- K. Choi, T. Y. Hou, A. Kiselev, G. Luo, V. Sverak, and Y. Yao *On the Finite-time Blowup of a 1D Model fro the 3D Axisymmetric Euler Equations*, arXiv:1407.4776v2 [math.AP].
- T. Y. Hou and P. Liu, *Self-Similar Singularity for a 1D Model of the 3D Axisymmetric Euler Equations*, Research in Mathematical Sciences, Vol. 2, No. 5, pp. 1-26, 2015. DOI 10.1186/s40687-015-0021-1.